

LOCKHEED MARTIN ENERGY RESEARCH LIBRARIES



3 4456 0515825 4

CENTRAL RESEARCH LIBRARY
DOCUMENT COLLECTION

Cy 1

ORNL-4246

UC-25 - Metals, Ceramics, and Materials

RADIATION METALLURGY SECTION

SOLID STATE DIVISION

PROGRESS REPORT

FOR PERIOD ENDING JANUARY 1968

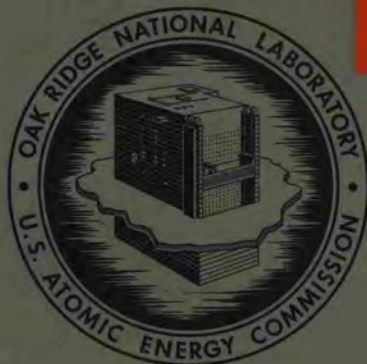
OAK RIDGE NATIONAL LABORATORY
CENTRAL RESEARCH LIBRARY
DOCUMENT COLLECTION

LIBRARY LOAN COPY

DO NOT TRANSFER TO ANOTHER PERSON

If you wish someone else to see this
document, send in name with document
and the library will arrange a loan.

UCN-7969
13 3-671



OAK RIDGE NATIONAL LABORATORY

operated by

UNION CARBIDE CORPORATION

for the

U.S. ATOMIC ENERGY COMMISSION

Printed in the United States of America. Available from Clearinghouse for Federal
Scientific and Technical Information, National Bureau of Standards,
U.S. Department of Commerce, Springfield, Virginia 22151
Price: Printed Copy \$3.00; Microfiche \$0.65

LEGAL NOTICE

This report was prepared as an account of Government sponsored work. Neither the United States, nor the Commission, nor any person acting on behalf of the Commission:

- A. Makes any warranty or representation, expressed or implied, with respect to the accuracy, completeness, or usefulness of the information contained in this report, or that the use of any information, apparatus, method, or process disclosed in this report may not infringe privately owned rights; or
- B. Assumes any liabilities with respect to the use of, or for damages resulting from the use of any information, apparatus, method, or process disclosed in this report.

As used in the above, "person acting on behalf of the Commission" includes any employee or contractor of the Commission, or employee of such contractor, to the extent that such employee or contractor of the Commission, or employee of such contractor prepares, disseminates, or provides access to, any information pursuant to his employment or contract with the Commission, or his employment with such contractor.

ORNL-4246

Contract No. W-7405-eng-26

RADIATION METALLURGY SECTION
SOLID STATE DIVISION
PROGRESS REPORT
For Period Ending January 1968

D. S. Billington, Director, Solid State Division
M. S. Wechsler, Head, Radiation Metallurgy Section

APRIL 1968

OAK RIDGE NATIONAL LABORATORY
Oak Ridge, Tennessee
Operated by
UNION CARBIDE CORPORATION
for the
U. S. ATOMIC ENERGY COMMISSION

LOCKHEED MARTIN ENERGY RESEARCH LIBRARIES



3 4456 0515825 4



CONTENTS

Summary.	v
Radiation Metallurgy	1
Introduction	1
The Temperature Dependence of Yielding in an Irradiated Pressure-Vessel Steel and the Relationship Between Radiation Hardening and Embrittlement	6
Introduction	6
Experimental Details	9
Results	12
Discussion.	20
Post-Irradiation Annealing of ASTM A-212-B Steel	27
Strain Aging of Neutron Irradiated Steel	30
Experimental Procedures and Results	31
Effect of Thermal Neutrons on the Tensile Properties of ASTM A-212-B and A-302-B Steels.	36
Properties of 12-Inch-Thick ASTM A-533-B, Class I, Steel	38
The Interaction Between Oxygen and Radiation-Produced Defects in Niobium	42
Introduction	42
Results	43
Discussion	47
Trapping of Oxygen and Nitrogen in Neutron-Irradiated Vanadium	51
The Annealing Characteristics of Neutron Irradiated Niobium	55
Experimental Procedures.	56
Tensile Results	57
Transmission Electron Microscopy	59
Discussion	64
Fluence Dependence of Radiation Hardening in Polycrystalline Niobium	66
Introduction.	66
Experimental Details	69
Results	70
Discussion	72
Deformation of Irradiated and Unirradiated Nb Single Crystals in Compression	75

Spark-Machining Damage in Niobium Single Crystals as Indicated by Etch Figures	84
Evaluation of Niobium Source Materials Suitable for Electron Beam Float Zone Melting	89
Experimental Procedure.	90
Experimental Results	94
Discussion	100
Conclusions	104

SUMMARYOAK RIDGE NATIONAL LABORATORY - SOLID STATE DIVISION

Investigations into radiation damage, hardening, and embrittlement in the body-centered cubic metals are continuing. This report covers recent work on pressure vessel steels, niobium, and vanadium.

Tensile and impact samples of a particular heat of ASTM A-212-B steel have been irradiated in the same facility in the Oak Ridge Research Reactor to the same fluence and at the same temperature. The samples were tested over a range of temperatures from about 30°K to 473°K and, for the tensile samples, at several strain rates. The yield stress increased strongly with decreasing test temperature, but the increase in yield stress upon irradiation was largely the same for all test temperatures. Strain rate and triaxiality corrections were applied to the tensile data in order to evaluate yield conditions near the root of the notched-bar impact samples. The ductile-brittle transition temperature under notch-impact loading for unirradiated and irradiated steel was found to be consistent with a simple criterion for brittle fracture. However, it was necessary to assume that cleavage crack initiation occurs at a point of lower triaxiality (closer to the root of the notch) in the irradiated steel.

Annealing and strain aging experiments on irradiated steel were also conducted, which indicate the effect of the trapping of interstitial elements at radiation-produced defect clusters.

In order to determine whether thermal neutrons have an effect on the radiation hardening of ASTM A-212-B and A-302-B steels, tensile samples were irradiated with and without cadmium shielding. No

difference in the radiation hardening was detected, in agreement with similar previous experiments on Charpy impact samples.

Mechanical property tests are described on samples taken from a 12-inch-thick plate of ASTM A-533-B steel.

Internal friction and electrical resistivity measurements have revealed the trapping of interstitial elements (chiefly oxygen and nitrogen) in neutron-irradiated niobium and vanadium. For niobium, the temperatures for the dissociation of interstitial elements from the traps have also been determined.

Various aspects of radiation hardening in niobium are described. Transmission electron microscopy was used to detect the density and size distribution of defect clusters observed upon irradiation and upon post-irradiation annealing. The extent to which these may be correlated with radiation hardening and radiation-anneal-hardening is discussed. A discussion is also given of experiments on the fluence and temperature dependence of radiation hardening in niobium.

Finally, work is described bearing on the techniques of preparation and evaluation of niobium materials.

RADIATION METALLURGY

Solid State Division
Oak Ridge National Laboratory
Oak Ridge, Tennessee

D. S. Billington and M. S. Wechsler

INTRODUCTION - M. S. Wechsler

The Radiation Metallurgy Section is studying radiation damage, hardening, and embrittlement in the body-centered cubic metals. Despite a fairly large body of research results,¹ many important aspects of these phenomena are not well understood. For example, although the hardening and embrittlement are known to be due to radiation-produced defect clusters, the structure and size range of clusters most effective in increasing the strength and decreasing the ductility of metals have not been determined. While the questions of defect clusters and their effect on plastic deformation and fracture may seem to some to be only of academic interest, they are at the core of the problem of the radiation embrittlement of reactor pressure vessel steels.² The failure of a reactor pressure vessel could have catastrophic consequences to the public safety, and letters^{3,4} from the Advisory Committee on Reactor

¹M. S. Wechsler, "Radiation Embrittlement of Metals and Alloys," in The Interaction of Radiation with Solids, edited by R. Strumane et al., North Holland Publishing Co., Amsterdam, 1964, 296-345.

²M. S. Wechsler, "Radiation Damage to Pressure Vessel Steels," Nucl. Safety, 8, 461, (1967).

³J. P. Blakely, "ACRS Comments on Reactor-Safety Research," Nucl. Safety, 8, 277, (1967).

⁴"Text of ACRS Letter to AEC," Nucleonics, 24, 17, (1966).

Safeguards to the Chairman of the Atomic Energy Commission have emphasized the advisability of certain research and development programs to develop pertinent information. The program of the Radiation Metallurgy Section⁵ is based on the premise that an assessment of the danger to reactor systems by virtue of the radiation embrittlement of structural metals and the ability to minimize this danger in the future are aided by a better understanding of the nature of the phenomenon itself. This requires a broad investigation that embraces fundamental and applied aspects of the problem.

The principal metals under investigation are pressure vessel steels, iron and iron alloys, niobium, and vanadium. As is characteristic of body-centered cubic metals, these metals exhibit a ductile-brittle transition and the ductile-brittle transition temperature (DBTT) is increased upon irradiation. The question arises as to whether this radiation embrittlement is chiefly a consequence of the radiation hardening or whether a change in the cleavage stress required to initiate a running cleavage crack is also important. To test this point for the pressure vessel steels we are conducting tensile and impact tests on samples from the same heat of steel irradiated under identical conditions. The results described below suggest that the increase in the DBTT can be correlated with the intersection of the yield curve (lower yield stress vs test temperature) and a critical cleavage stress.

⁵M. S. Wechsler, The Program of the Radiation Metallurgy Section, Solid State Division, Oak Ridge National Laboratory, ORNL-TM-2059, (1968).

The correlation does not require a decrease in the critical cleavage stress upon irradiation. However, it is necessary to assume that the degree of stress triaxiality at the point of cleavage fracture initiation is reduced in the irradiated steel.

The annealing characteristics of irradiated steel are also described below. The shape of the stress-strain curve (e.g., whether a yield drop is observed or not) is shown to depend on whether a short time-low temperature or a long time-high temperature annealing treatment is applied. This observation suggests that the annealing process occurs in several stages, and we deduce from the changes in the shape of the stress-strain curve during annealing that rearrangements in the distribution of interstitial elements are involved. Interstitial elements are also responsible for strain-aging effects, and thus, it was of interest to investigate the effect of neutron irradiation on strain aging in these steels. The results described below indicate that the strain aging is reduced after irradiation, probably due to the trapping of carbon and nitrogen at radiation-produced defect clusters.

One of the ACRS letters³ commented on the importance of research into thick-section and higher-strength steels and a Heavy Section Steel Technology Program⁶ is underway with the purpose of evaluating the application of such steels to nuclear pressure vessels. Under this program, some initial results have been obtained on samples from a 12-inch-thick plate of ASTM A-533-B steel.

⁶ F. J. Witt, Heavy Section Steel Technology Program Progress Report, ORNL-4176, (1968).

The notion of trapping of interstitial elements in irradiated BCC metals has received support from measurements of internal friction and electrical resistivity in irradiated niobium. The internal friction measurements are especially helpful since they are selective, i.e., from the frequency and temperature at which the internal friction is observed, one can deduce the amount of a particular interstitial element in solid solution. In this way, a fairly unambiguous determination was made of the trapping at about 150°C of oxygen in neutron-irradiated niobium.⁷ In this report, additional experiments are described in which the annealing was taken to higher temperatures at which the oxygen becomes dissociated from the traps and returns again to solid solution.

Vanadium is chemically similar to niobium and the trapping of interstitial elements at radiation-produced defects is also being investigated for this BCC metal. The results to date indicate that oxygen and nitrogen are trapped at temperatures between 150°C and 300°C, but the temperature range for the dissociation of the interstitials from defect traps has not yet been determined.

We have mentioned that the structure and size of the defect clusters that are critical to the radiation hardening have not yet been established. To help clarify this matter, an investigation is underway into the correlation between the size distribution of clusters in niobium observed by transmission electron microscopy and the changes in yield

⁷J. M. Williams, W. E. Brundage, and J. T. Stanley, "The Effect of Oxygen on 'Stage III' Annealing in Neutron-Irradiated Niobium," to be published in Metals Science Journal.

stress upon irradiation and upon post-irradiation annealing. The observed initial increase in yield stress upon irradiation is found to be consistent with a hardening model in which the radiation-produced defect clusters observed in the electron microscope are the hardening agents. However, the further increase in yield stress upon annealing cannot be accounted for by the size distribution of defect clusters and, therefore, it is suggested that interstitial carbon atoms migrate to the clusters and form even stronger barriers to dislocation motion. Also, the fluence dependence of the hardening indicates that the rate of hardening decreases with increasing fluence more rapidly than would be predicted by a dispersed barrier model. This "saturation effect" has been observed for other metals and remains one of the difficult questions in the understanding of radiation hardening.

The effect of radiation on the temperature dependence of yielding has been presented earlier for tensile tests on single crystals of niobium oriented for $\{110\} \langle 111 \rangle$ slip.⁸ In the present report, compression tests are reported for irradiated single crystals of the same orientation but somewhat higher purity. The irradiation appears to have introduced more temperature dependence for the higher purity samples, but this point needs further confirmation.

Finally, several aspects of our work on the preparation and evaluation of niobium sample material are described below.

⁸S. M. Ohr, R. P. Tucker, and M. S. Wechsler, "Radiation Hardening in B.C.C. Metals Niobium and Iron," in Proceedings of the International Conference on Strength of Metals and Alloys, Japan Inst. of Metals, (1968).

The Temperature Dependence of Yielding in an Irradiated Pressure-Vessel Steel and the Relationship Between Radiation Hardening and Embrittlement

M. S. Wechsler, N. E. Hinkle, R. G. Berggren, and W. J. Stelzman

Introduction

It is commonly recognized that yield and fracture in metals are intimately inter-related. Among other things, this is suggested by the fact that the ductile-brittle transition phenomenon is exhibited by the BCC metals which are the very materials that show strong temperature dependence of yielding. The exact nature of the relationship between flow and fracture is complicated by many material and testing variables. Nevertheless, a useful first approximation to the relationship was expressed over a quarter-century ago by the principles formulated by Mesnager, Ludwig, Davidenkov, and Wittman (cf. Orowan,⁹ Tetelman and McEvily¹⁰). These principles, illustrated in Fig. 1, suggest that the ductile-brittle transition occurs at the temperature where the appropriate yield stress, σ_y , and fracture stress, σ_c , curves intersect. It is emphasized that σ_y and σ_c are quantities appropriate to the material and type of test. For example, for the ductile-brittle transition temperature (DBTT) obtained by Charpy V-notch impact tests on a pressure-vessel steel, the σ_y should refer to the yield stress under the actual conditions of strain rate and stress state of the impact test and the σ_c should be

⁹E. Orowan, "Classical and Dislocation Theories of Brittle Fracture," Fracture, Wiley, New York, 147, (1959).

¹⁰A. S. Tetelman and A. J. McEvily, Fracture of Structural Materials, John Wiley and Sons, New York, (1967).

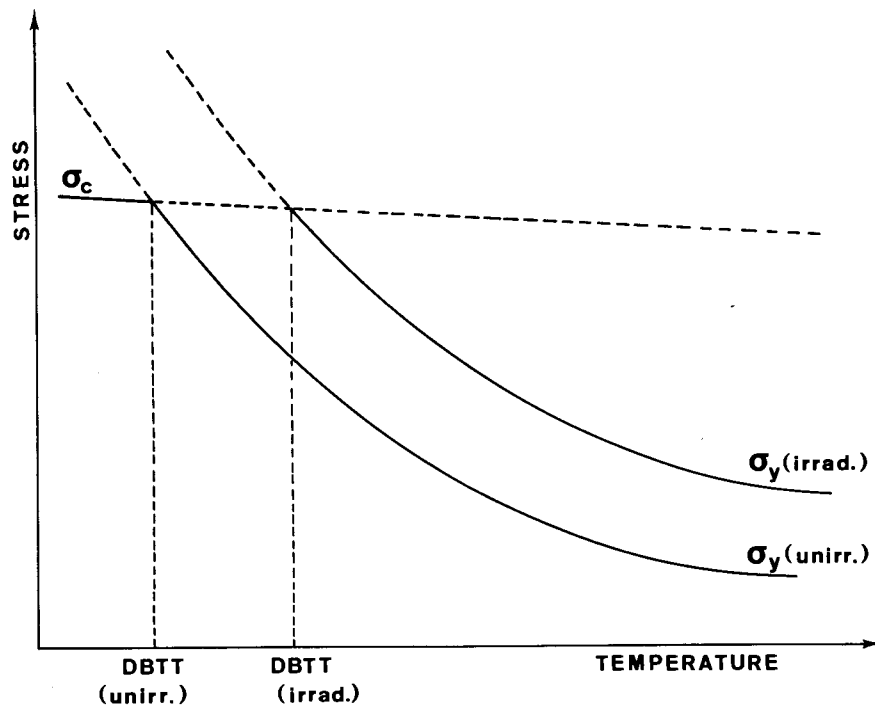


Fig. 1. Schematic Illustration of the Relationship Between the Increase Upon Irradiation of Yield Stress (σ_y) and Ductile-Brittle Transition Temperature (DBTT).

the effective cleavage fracture stress of the material, given all its eutectoid decomposition products, inclusions, and the like. Armstrong^{11,12} has applied these ideas to the influence of grain size on the DBTT of steels and has expressed the DBTT analytically in terms of experimentally determined quantities. Also, Hendrickson, Wood, and Clark^{13,14}

¹¹R. W. Armstrong, "On Determining the Ductile-Brittle Transition Temperature," Phil. Mag., 9, 1063, (1964).

¹²R. W. Armstrong, "Stress-Grain Size Analysis of the Brittle Fracture Transition of Steel," ARPA E 38, February (1967).

¹³J. A. Hendrickson, D. S. Wood, and D. S. Clark, "The Initiation of Brittle Fracture in Mild Steel," Trans. ASM, 50, 656, (1958).

¹⁴J. A. Hendrickson, D. S. Wood, and D. S. Clark, "Prediction of Transition Temperature in a Notched Bar Impact Test," Trans. ASM, 51, 629, (1959).

have conducted notch-tensile and notch-impact tests on a mild steel as a function of test temperature and strain rate. Their results constitute an experimental verification of the concepts, since they found that a necessary and sufficient condition for the occurrence of brittle fracture was the attainment of a critical tensile stress, σ_c , before yielding occurred across the specimen.

This approach provides a useful clue to the understanding of the origin of radiation embrittlement. As is illustrated in Fig. 1, since the yield stress of irradiated metals is increased, the point of intersection between σ_y and σ_c is shifted upwards on the temperature scale, thus increasing the DBIT. The question arises as to whether the increase in σ_y is in itself sufficient to account for the Δ DBIT upon irradiation assuming no change in σ_c , or whether the σ_c is also changed in the irradiated material. In most discussions of the problem along these lines (cf. Armstrong,^{11,12} Tetelman and McEvily¹⁰), σ_c is assumed to be rather independent of temperature and strain rate. Hendrickson, et al.^{13,14} concluded from their experiments that σ_c is independent of temperature and strain rate, whereas Wilshaw and Pratt¹⁵ observed some variation. However, little is known concerning the effect of radiation on σ_c . Based on criteria described below, we find a slight increase in σ_c upon irradiation.

A strict test of these ideas is difficult to make because of the necessity of doing tests as a function of temperature, strain rate, and

¹⁵T. R. Wilshaw and P. L. Pratt, "The Effect of Temperature and Strain-Rate on the Deformation and Fracture of Mild-Steel Charpy Samples," Proc. First International Conference on Fracture, 2, 973, (1966).

stress state on materials identical in every respect except the irradiation treatment. In this report, we describe an attempt to do this on un-irradiated and irradiated ASTM A-212-B pressure-vessel steel on which tensile and impact tests were performed as a function of temperature and, to a limited extent, strain rate. The results are interpreted in terms of Fig. 1 on the assumption that σ_c is independent of temperature and strain rate. The observations suggest that the σ_c is increased slightly by the irradiation and the degree of triaxiality reached in the Charpy test at the point where cleavage is initiated is decreased slightly. When these changes are taken into consideration, the DBTT's for smooth tensile and notch impact tests are predicted reasonably well on the basis of the Mesnager-Ludwig-Davidenkov-Wittman approach.

Experimental Details

The material for this study was taken from the quarter thickness plane of a 2 3/4 inch plate of ASTM A-212-B pressure vessel steel. This plate, originally fabricated for the EGCR pressure vessel, was rolled from an aluminum-treated heat of steel melted according to fine-grain practice. The mill chemical analysis and specifications are given in Table 1. The plate was normalized at about 900°C (1650°F), water-spray cooled to 260°C (500°F), and stress relieved at 650-680°C (1200-1250°F). The ferrite grain diameter was about 20 micron (ASTM grain size No. 9).

The tensile samples were machined to a gage length of 1.25 inch and a gage diameter of 0.177 inch. The tensile tests were performed on an Instron testing machine. The tensile samples were held in slotted-type grips with the load exerted on the smooth fillets at the ends of

TABLE I

Mill Report on ASTM A-212 Grade B Steel Plate

SSD Item No.	157
Heat No.	A-2056
Thickness	2 3/4 in.
Carbon	0.27%
Maganese	0.70%
Phosphorus	0.012%
Sulphur	0.032%
Silicon	0.20%
Yield Strength	45,200 psi
Ultimate Tensile Strength	75,900 psi
Elongation in 2"	28%

the gage length. The test temperatures from room temperature to 77°K (-196°C) were obtained by spraying liquid nitrogen or cold nitrogen gas uniformly over the sample, grips, and pull rods. The low temperature tensile apparatus used in this study was an adaptation of the system used by Spreadborough, et al.¹⁶ The test chamber consisted of a series of small diameter tubes arranged parallel to and equally spaced around the pull rods, and a styrofoam insulating shell around the spray tubes. Each tube had small holes drilled through the surface facing the pull rods such that nitrogen forced through the tubes was sprayed toward the pull rods. Below 77°K, liquid helium was forced through a vacuum insulated tube and sprayed over the sample after precooling the assembly to 77°K. Temperatures above room temperature were obtained by placing

¹⁶J. Spreadborough, et al, "The Effect of Radiation on the Ductile-Brittle Transition in Pressure Vessel Steels," Final Report EUR-2354E, EURAC 1394, (1965).

a ceramic clam-shell furnace insert around the sample and grips. Temperatures were measured with copper-constantan thermocouples attached to the sample and the grips. The thermocouples were calibrated at liquid nitrogen and liquid helium temperatures. National Bureau of Standards tables of emf vs. temperature were used for temperatures above 77°K. Below 77°K, a computed table of emf vs. temperature compiled by Adams and Davisson¹⁷ was used.

The impact samples were prepared from the same heat of steel as the tensile samples (Table 1) and conformed to ASTM specifications for standard Charpy V-notch impact tests. The impact machine was equipped with a temperature conditioning chamber containing carbon electrodes for resistance heating, a liquid nitrogen line for cooling, and a spring-loaded contact thermocouple for temperature measurement. The samples were transferred from the chamber to the test position by a pneumatic cylinder and located in test position by three pneumatic cylinders. Interlocks prevented dropping of the pendulum hammer until transfer and locating devices were retracted. The elapsed time from time of removal from the temperature chamber to the time of impact was less than three seconds.

The irradiations were performed at the poolside facility of the Oak Ridge Research Reactor where the fluence rate was $(2-3) \times 10^{12} \text{n/cm}^2 \cdot \text{sec}$ ($E > 1 \text{ Mev}$). The tensile and impact samples were irradiated at 60°C to fluences of 10 and 9.8×10^{18} neutrons/cm² ($E > 1 \text{ Mev}$), respectively.

¹⁷R. K. Adams and E. G. Davisson, "Smoothed Thermocouple Tables of Extended Significance (°C)," 2, Section 2.11, Constantan Copper Cryogenic Thermocouples, ORNL-3649, 2, March (1965).

Results

A. Tensile Tests

The tensile samples were tested at two strain rates, 2.7×10^{-4} and $2.7 \times 10^{-2} \text{ sec}^{-1}$. At $2.7 \times 10^{-4} \text{ sec}^{-1}$ the testing temperatures covered the range from about 20°K to 473°K for the unirradiated samples. Fewer tests were conducted below 77°K for the irradiated samples, and the maximum temperature was 373°K . The irradiated samples exhibited the usual increase in yield stress, decrease in rate of work hardening, and decrease in uniform and fracture elongations, as is seen in Fig. 2 showing load-extension curves taken at 77, 133, and 299°K .

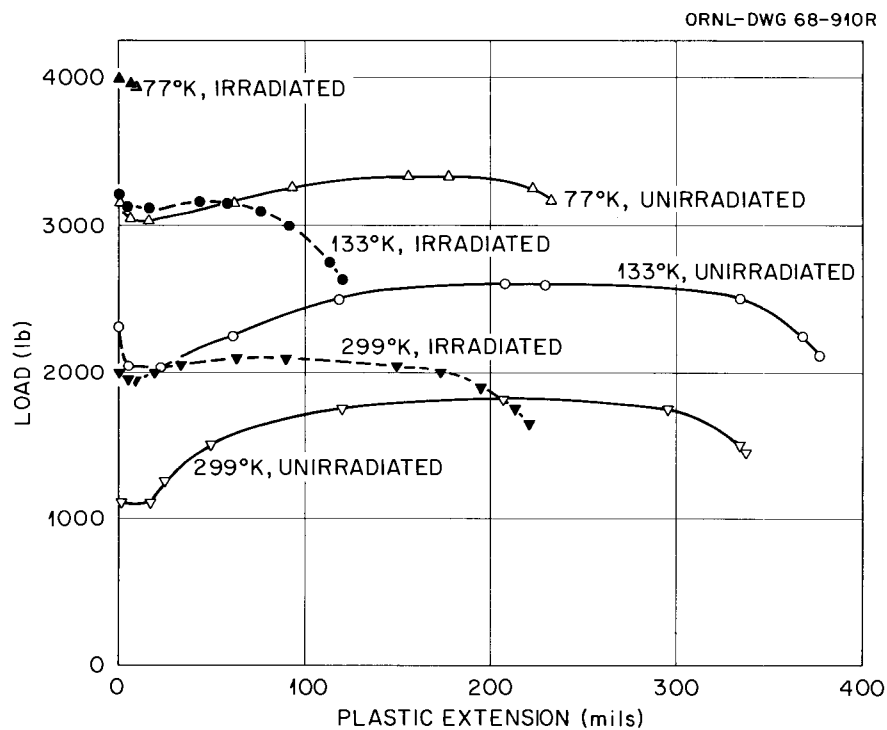


Fig. 2. Load-Extension Curves for Unirradiated and Irradiated ($\Phi = 1.0 \times 10^{19} \text{ n/cm}^2$, 60°C) A-212-B Steel Tested at 77, 133, and 299°K at Strain Rate of $2.7 \times 10^{-4} \text{ sec}^{-1}$.

The effect of irradiation on the yield properties as a function of test temperature is shown in Fig. 3. With decreasing test temperature, the unirradiated yield stresses increase quite rapidly and the rate of work hardening decreases as is suggested by the approach of the UTS curve toward the LYS and UYS curves. The increase in yield stress upon irradiation to 1×10^{19} n/cm² ($E > 1$ Mev) is largely independent of temperature from 373°K to 60°K. This was also observed by Chow, McRickard, and Gurinsky¹⁸ for A-212-B tensile samples irradiated to 2×10^{18} n/cm² ($E > 1$ Mev) and tested over a comparable range of temperatures and by Fearnough¹⁹ for a variety of notched steel bars irradiated to $10^{19} - 10^{20}$ n/cm² and tested down to about 190°K. The true fracture stress shows a sharp decrease at 70-80°K for the unirradiated steel, similar to that observed by Hahn, et al.²⁰ At this temperature they observed that the frequency of microcracks in the microstructure begins to rise. Thus, we may use the intersection of the fracture stress (FS) and lower yield stress (LYS) curves in Fig. 3 as a measure of the DBTT for uniaxial tension of smooth samples. This occurs at the intersection of arrows A and B giving 56°K for the DBTT under these conditions and 153 kpsi for the cleavage fracture stress, σ_c . At temperatures below about 60°K the lower yield is never reached, the sample

¹⁸J. G. Y. Chow, S. B. McRickard, and D. H. Gurinsky, "Mechanical Properties of Irradiated Iron and Iron Alloys," in Symposium on Radiation Effects on Metals and Neutron Dosimetry, ASTM-STP-341, American Society for Testing and Materials, Philadelphia, 46, (1963).

¹⁹G. D. Fearnough, "The Strain Rate Sensitivity of the Yield Stress of Steels," in The Physical Basis of Yield and Fracture, Oxford, Institute of Physics and Physical Society, 88, (1966).

²⁰G. T. Hahn, B. L. Averbach, W. S. Owen, and M. Cohen, "Initiation of Cleavage Microcracks in Polycrystalline Iron and Steel," in Fracture, Oxford, Institute of Physics and Physical Society, 91, (1966).

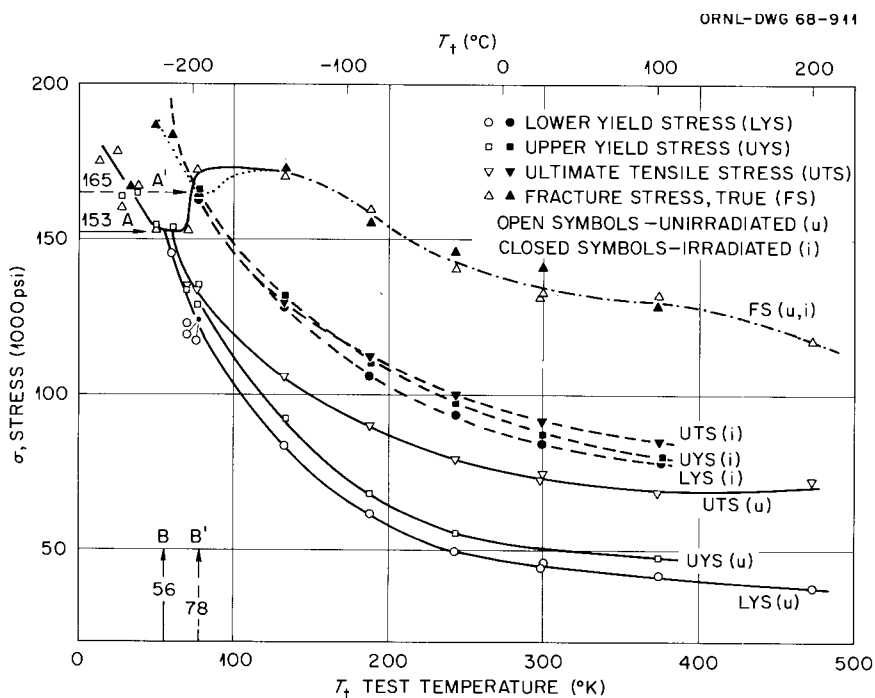


Fig. 3. Stress vs Test Temperature for Unirradiated and Irradiated ($\Phi = 1.0 \times 10^{19}$ n/cm², 60°C) A-212-B Tested at Strain Rate of 2.7×10^{-4} sec⁻¹.

exhibiting brittle fracture at or slightly after the UYS is reached or even prior to reaching the upper yield point.

The FS for the irradiated material does not show the large decrease as the DBTT is approached, although fewer points are available to define its shape in the lower temperature region. However, as suggested in Fig. 3 it appears that the FS and LYS curves intersect at 78°K and 165 kpsi, thus defining the DBTT and σ_c corresponding to those discussed above. It is interesting that the FS curves for the unirradiated and irradiated steel do not appear to differ significantly at temperatures above the transition. However, Fig. 3 does show the reduced rate of work hardening in the irradiated material in that the UTS curve lies quite close to the curves for LYS and UYS.

Another measure of the transition from ductile to brittle behavior is the reduction of area (RA) at fracture. This is shown in Fig. 4 as a sharp drop near the DBTT. Extrapolating the RA curves to the abscissa, we can identify the DBTT's as 70°K and 81°K for the unirradiated and irradiated samples, respectively, in fair agreement with the temperatures 56 and 78°K determined in Fig. 3. Fig. 4 also shows that RA curves for unirradiated and irradiated conditions approach each other as the test temperature is increased.

The curves in Fig. 5 show the transition behavior of the uniform strain. For the unirradiated samples, the transition temperature is fairly well defined at 62°K, but the points for the irradiated samples are not as plentiful and we can only state that the irradiated transition is above 77°K and below about 130°K.

A number of authors have commented on the shape of the LYS curve as a function of test temperature. We find that an adequate fit to the observations is given by an equation of the form discussed by McKinsey, et al.,²¹ namely,

$$\sigma = \sigma_0 + \frac{B}{T_t} \quad (1)$$

A least-squares fit to the LYS for unirradiated samples gives $\sigma_0 = 21.5 \pm 2.2$ kpsi and $B = (7.5 \pm 0.2) \times 10^3$ kpsi·deg K; the comparison with observed values is shown in Fig. 6. For the irradiated samples, the parameters in Eq. (1) were chosen in two ways: (1) for best general fit as for the unirradiated samples; this gives $\sigma_0 = 59.4 \pm 3.7$ kpsi and

²¹C. R. McKinsey, A. L. Mincher, W. F. Sheely, and J. L. Wilson, "Investigation of Tungsten-Tantalum-Columbium-Base Alloys," ASD Technical Report 61-3, July (1961).

$B = (8.3 \pm 0.5) \times 10^3$ kpsi·deg K, and (2) best fit assuming no change in the temperature dependence upon irradiation, i.e. assuming $B = 7.5 \times 10^3$ kpsi·deg K as before; this gives $\sigma_0 = 64.0$ kpsi. The curves for cases (1) and (2) are also plotted in Fig. 6. It would appear that B is increased slightly upon irradiation, but the increase is barely outside experimental error. This may be seen in Fig. 6 in that curves (1) and (2) appear to be almost equally good fits to the experimental points.

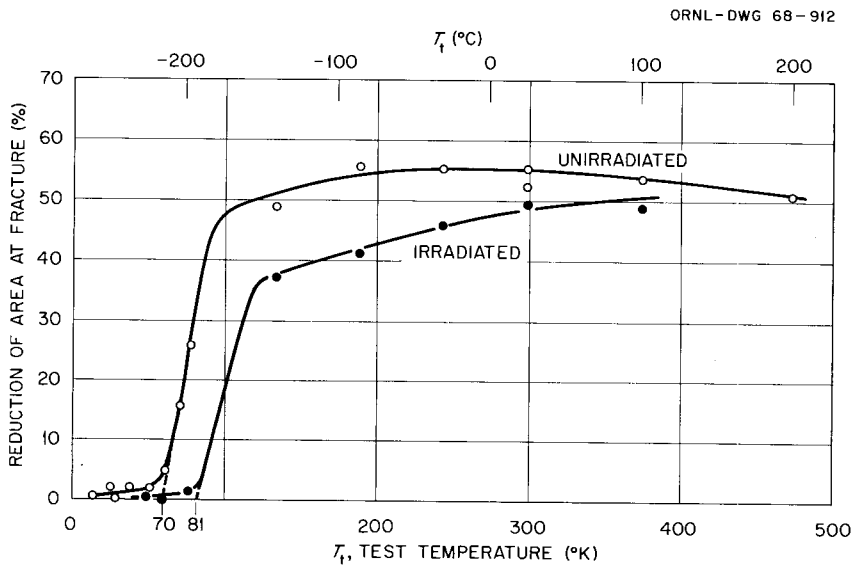


Fig. 4. Reduction of Area at Fracture vs Test Temperature for Unirradiated and Irradiated ($\Phi = 1.0 \times 10^{19}$ n/cm², 60°C) A-212-B Steel Tested at Strain Rate of 2.7×10^{-4} sec⁻¹.

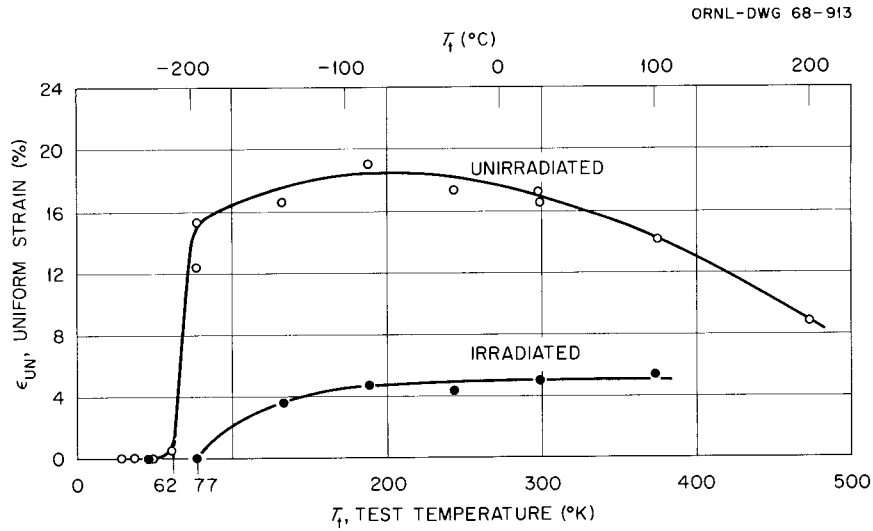


Fig. 5. Uniform Strain vs Test Temperature for Unirradiated and Irradiated ($\Phi = 1.0 \times 10^{19}$ n/cm², 60°C) A-212-B Steel Tested at Strain Rate of 2.7×10^{-4} sec⁻¹.

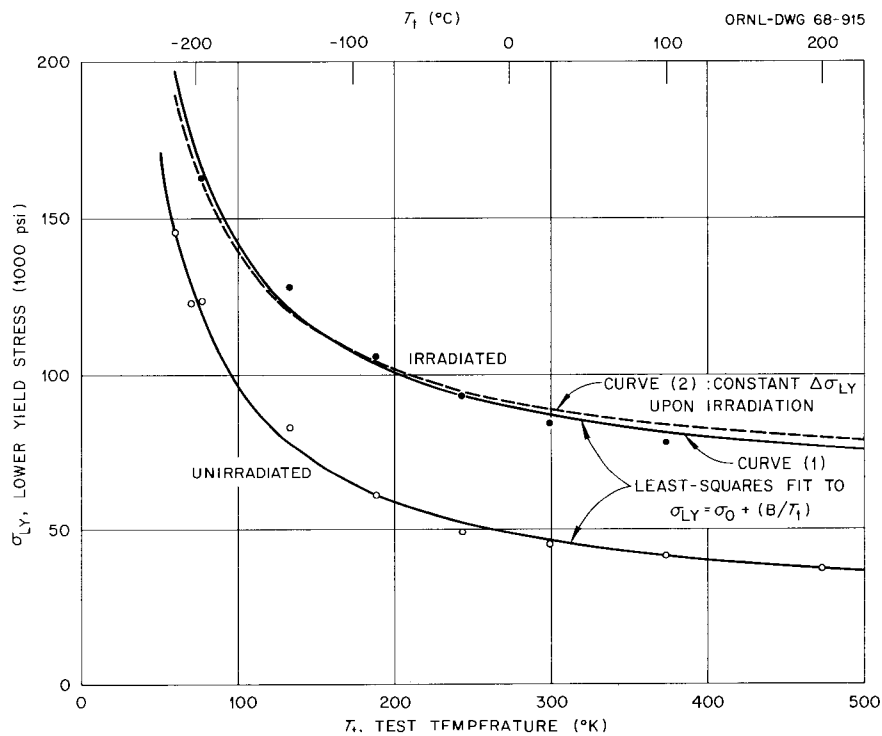


Fig. 6. Lower Yield Stress vs Test Temperature for Unirradiated and Irradiated ($\Phi = 1.0 \times 10^{19}$ n/cm², 60°C) A-212-B Steel Tested at Strain Rate of 2.7×10^{-4} sec⁻¹. Illustration of the fit to $\sigma_{LY} = \sigma_0 + (B/T_t)$.

It is of course of interest to know at what microstructural feature or features the cracking is initiated at low temperatures. Figures 7 and 8 show photomicrographs at 1000X and 2000X for an unirradiated sample tested to fracture at 28°K. The photographs indicate cracks in the longitudinal section near the fracture surface. The fracture path is oriented in a variety of ways relative to grain boundaries, pearlite colonies, and twin bands, and these photographs do not appear to suggest a special significance to any one type of feature.



Fig. 7. Photomicrograph at 1000X of Longitudinal Section (Stress Axis Vertical) of Unirradiated sample of A-212-B Steel Tested to Fracture at 28°K. Nital (2%) Etch.



A



B

Fig. 8. Photomicrographs at 2000X of Longitudinal Section (Stress Axis Vertical) of Unirradiated Sample of A-212-B Steel Tested to Fracture at 28°K. Nital (2%) Etch. (a) Oblique Light; (b) Direct Light.

A limited number of tensile tests were conducted on unirradiated samples at a strain rate of $2.7 \times 10^{-2} \text{ sec}^{-1}$ in the temperature range between 77 and 299°K. However, in what follows we shall refer only to measurements at 188, 243, and 299°K. This is done in the Discussion section below.

B. Impact Tests

The impact tests were conducted over a range of temperatures from -75°C (198°K) to 175°C (448°K) and the results were expressed in terms of the fracture energy and the fracture appearance. Figure 9 indicates that the irradiation to 9.8×10^{18} neutrons/cm² ($E > 1 \text{ Mev}$) increased the DBTT under notched-bar impact conditions from 5°C to 108°C on the basis of a 20 ft-lb fracture energy criterion and from -30°C to 65°C based on the criterion of nil fibrous fracture appearance. The latter criterion appears more in accord with the reduction-in-area criterion (Fig. 4) adopted for the smooth tensile samples; therefore in the discussion that follows, we will use -30°C (243°K) and 65°C (338°K) for the unirradiated and irradiated notched-bar impact DBTT's, respectively, as determined from the fracture appearance curves in Fig. 9 and listed in Table 2.

Discussion

As was mentioned in the Introduction, our object is to see to what extent it is possible to apply the simple concept enunciated by Mesnager, Ludwig, Davidenkov, and Wittman (Fig. 1) to the radiation embrittlement of pressure vessel steels. At the outset, an effective cleavage stress,

σ_c , must be adopted. Based on the intersection of the yield stress and fracture stress curves (Fig. 3), values of $\sigma_c = 153$ kpsi and 165 kpsi were chosen for the unirradiated and irradiated material, respectively. The DBTT's under low-strain-rate, smooth-tensile conditions deduced from Fig. 3 were 56°K (unirradiated) and 78°K (irradiated). These agree reasonably well with the DBTT's of 70°K (unirradiated) and 81°K (irradiated) observed for the reduction of area at fracture (Fig. 4 and Table 2) and the DBTT's of 62°K (unirradiated) and 77-130°K (irradiated) observed for the uniform strain (Fig. 5 and Table 2).

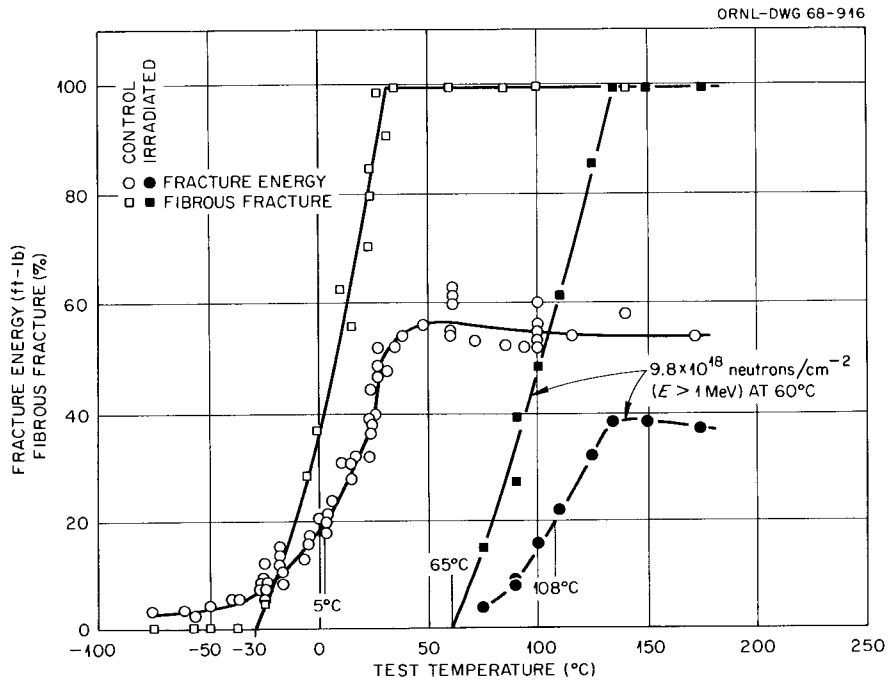


Fig. 9. Effect of Neutron Irradiation on Charpy V-Notch Impact Tests on Unirradiated and Irradiated ($\Phi = 9.8 \times 10^{18}$ n/cm², 60°C) A-212-B Steel.

Table 2. Ductile-Brittle Transition Temperatures (DBTT) for Unirradiated and Irradiated ($\Phi = 1.0 \times 10^{19}$ n/cm², 60°C) A-212-B Steel

Criterion and Type of Test	DBTT Unirrad.	DBTT Irrad.
1. Intersection of fracture and yield curves, smooth tensile, $\dot{\epsilon} = 2.7 \times 10^{-4}$ sec ⁻¹ (Fig. 3)	56°K	78°K
2. Nil reduction of area at fracture, smooth tensile, $\dot{\epsilon} = 2.7 \times 10^{-4}$ sec ⁻¹ (Fig. 4)	70°K	81°K
3. Nil uniform strain, smooth tensile, $\dot{\epsilon} = 2.7 \times 10^{-4}$ sec ⁻¹ (Fig. 5)	62°K	77-130°K
4. Fracture appearance, Charpy impact (Fig. 9)	243°K	338°K
5. Intersection of fracture and yield curves, notch impact, $\dot{\epsilon} = 2 \times 10^3$ sec ⁻¹ (Fig. 10)	223°K (K = 2.1)	338°K (K = 1.74)*

*K adjusted to give DBTT = 338°K.

On the assumption that σ_c is independent of temperature, the DBTT for a given type of test should occur where the appropriate yield curve, corrected for strain rate and triaxiality, reaches the value 153 kpsi or 165 kpsi for unirradiated or irradiated material, respectively. In Fig. 10 the yield and cleavage stress curves are shown for the unirradiated and irradiated steel. The observed unirradiated lower yield stress is shown at Curve (A) for $\dot{\epsilon} = 2.7 \times 10^{-4}$ sec⁻¹ and at Curve (B) for $\dot{\epsilon} = 2.7 \times 10^{-2}$ sec⁻¹. In order to derive the DBTT (unirradiated) under notch impact conditions, these curves must be corrected for the strain rate and triaxiality at the point of fracture below the root of the

notch. The notch-impact strain rate is estimated to lie in the range $(1.0 - 2.3) \times 10^3 \text{ sec}^{-1}$ and we shall use the value $2 \times 10^3 \text{ sec}^{-1}$ given by Wilshaw and Pratt.²² To make the extrapolation to this strain rate we apply a constant strain-rate-sensitivity factor, $\Delta \sigma / \Delta \ln \dot{\epsilon}$, as determined from the measurements at 2.7×10^{-4} and $2.7 \times 10^{-2} \text{ sec}^{-1}$. The extrapolated curve appropriate to unirradiated material at $2 \times 10^3 \text{ sec}^{-1}$ is labelled (C) in Fig. 10. At room temperature the measured yield stress at $2.7 \times 10^{-4} \text{ sec}^{-1}$ is 46 kpsi and this is calculated to be increased to 60 kpsi at $2 \times 10^3 \text{ sec}^{-1}$ or an increase of 14 kpsi. This may be compared with the results given by Fearnough (Ref. 19, Fig. 4) for the dynamic increase in yield stress as a function of the static yield stress. For a static yield stress of 46 kpsi (32 kg/mm^2), the increase in yield stress obtained from his instrumented Charpy tests is given as 15 kpsi (11 kg/mm^2).

A triaxiality correction must also be applied since the yielding is governed by the maximum shear stress, τ , whereas the cleavage fracture depends largely on the longitudinal stress, σ_{yy} , below the root of the notch. In the absence of triaxiality

$$\sigma_{yy} = 2\tau = \sigma_{LY}$$

whereas when the stress state is triaxial

$$\sigma_{yy} = K 2\tau$$

where K is the plastic stress concentration factor. The maximum possible value of K for a Charpy bar is 2.18 (Ref. 10, p. 296), and Wilshaw and

²²T. R. Wilshaw and P. L. Pratt, "The Effect of Temperature and Strain-Rate on the Deformation and Fracture of Mild-Steel Charpy Samples," Proc. First International Conference on Fracture, 2, 973, (1966).

Pratt²² obtained 2.05 ± 0.05 experimentally. Hence, for the unirradiated material we apply a triaxiality correction of 2.1; that is, we raise Curve (C) in Fig. 10 a factor of 2.1 to bring it to Curve (D). Curve (D) intersects the horizontal $\sigma_c = 153$ kpsi line at 223°K. Thus, the predicted DBTT (unirradiated) for notch-impact loading is 223°K to be compared with the observed value of 243°K deduced from the fracture appearance curve in Fig. 9. In view of the approximations inherent in the analysis, this may be considered to constitute reasonable agreement.

For the analysis of results for the irradiated samples, the same strain-rate correction was applied as for the unirradiated samples, bringing Curve (A') to (C') in Fig. 10. This seems reasonable in view of the slight change in temperature dependence upon irradiation (Fig. 6).

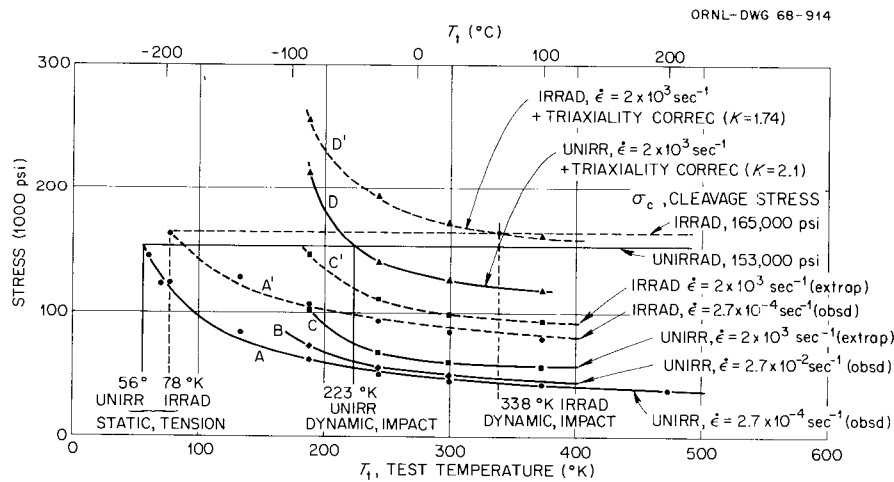


Fig. 10. Stress vs Test Temperature for Unirradiated and Irradiated ($\Phi = 1.0 \times 10^{19}$ n/cm², 60°C) A-212-B Steel.

Also, Campbell and Harding²³ and Fearnough²⁴ observed little change upon irradiation in the rate sensitivity of steels tested from 10^{-3} to 10^3 sec⁻¹. Figure 10 indicates that if the full triaxiality correction of 2.1 were applied to the irradiated case the predicted increase in DBTT upon irradiation would be too large. However, a decrease in the triaxiality correction from $K = 2.1$ to $K = 1.74$ allows the point of intersection of Curve (D') with the $\sigma_c = 165$ kpsi line to fall at 338°K , the DBTT obtained from the impact tests. The stress concentration factor is given in terms of distance, x , below the notch by^{25,22}

$$K = 1 + \ln \left(1 + \frac{x}{r} \right)$$

where r is the root radius, 0.25 mm. A decrease in K from 2.1 to 1.74 corresponds to a decrease in $\frac{x}{r}$ from 2.0 to 1.1.

Observations of the shapes of yield zones in steels^{22,23,26} by etching techniques have revealed the succession of events that takes place as deformation spreads from the surface across the specimen. At first the deformation is confined to a small plastic zone or wedge just below the notch root. But then a point of plastic instability is

²³J. D. Campbell and J. Harding, "Effect of Grain Size, Strain Rate, and Neutron Irradiation on Tensile Strength of α -Fe," in Response of Metals to High Velocity Deformation, 51, Interscience, N. Y. (1961).

²⁴G. D. Fearnough, "The Strain Rate Sensitivity of the Yield Stress of Steels," in The Physical Basis of Yield and Fracture, Oxford, Institute of Physics and Physical Society, 88, (1966).

²⁵A. S. Tetleman and A. J. McEvily, Fracture of Structural Materials, John Wiley and Sons, New York, (1967).

²⁶J. R. Griffiths and A. H. Cottrell, "Notch Effects on Slip, Twinning and Fracture in Silicon-Steel," J. Mech. Phys. Solids, 15, No. 2, 125-133, March, (1967).

reached at which far-reaching arcs or "hinges" of deformation sweep suddenly across the entire specimen section. A lower value of K associated with the DBTT (irradiated, notch impact) at 338°K in Fig. 10 implies that this plastic instability is reached closer to the surface for the irradiated material where the triaxiality is 1.74 instead of 2.1 .

Possibly this could be due to intensification of strain in the plastic zone due to the coarsening of slip characteristic of irradiated metals. On the other hand, it may be that the σ_c increases with temperature (and perhaps strain rate) in the irradiated steel. To account for the DBTT at 338°K using $K = 2.1$ as for the unirradiated case, the σ_c would have to increase from 165 kpsi at 78°K and $2.7 \times 10^{-4} \text{ sec}^{-1}$ to 200 kpsi at 338°K and $2 \times 10^3 \text{ sec}^{-1}$. If a similar increase in σ_c were permitted for the unirradiated steel, the DBTT would be decreased only slightly (from 223°K to 210°K). The relative insensitivity of the DBTT (impact, unirradiated) to variations in σ_c is a consequence of the fact that Curve (D), Fig. 10, is rising fairly steeply in the region of 200 - 250°K . On the other hand, for the DBTT (impact, irradiated) the slope of Curve (D') near 340°K is quite low and small changes in σ_c have a considerable effect upon the point of intersection with the yield curve, i.e. upon the DBTT.

One of the puzzling features of radiation embrittlement in the pressure vessel steels is the large variability in the increase in DBTT from one steel to another or even from heat to heat.²⁷ The origin

²⁷M. S. Wechsler, "Radiation Damage to Pressure Vessel Steels," Nucl. Safety, 8, 461, (1967).

of this variability may lie in the fact that the temperature dependence of the yield curve is small at temperatures near the irradiated DBTT.

Post-Irradiation Annealing of ASTM A-212-B Steel

R. G. Berggren, W. J. Stelzman, T. N. Jones, and M. S. Wechsler

We have previously reported^{28,29} the results of post-irradiation annealing studies on several heats of ASTM A-212-B carbon-silicon steel. The post-irradiation annealing of Charpy V-notch impact transition temperature was reported^{28,29} for specimens irradiated at 55 to 70°C and 233 to 474°C. The post-irradiation annealing of tensile properties was reported²⁸ for specimens irradiated at 230 to 300°C. The results of post-irradiation annealing studies presented in this report are from tensile tests of specimens irradiated at about 60°C in the Oak Ridge Research Reactor. These tensile test specimens were from the quarter thickness location of a 2 3/4-inch-thick plate from Lukens heat no. A-2056 (SSD Item 157).²⁸ All the tests were conducted at 27°C and a strain rate of 2.7×10^{-4} sec⁻¹.

The degree of recovery of radiation-induced increase of lower yield stress is shown in Fig. 11. In previous work, the times for 50% recovery were shown to decrease with decreasing irradiation temperature in the range 94 to 290°C (cf Ref. 30). The present work is consistent with that trend, since for our irradiation temperature of 60°C the annealing times are shorter than for the higher irradiation temperatures of the previous work.

²⁸R. G. Berggren, W. J. Stelzman, and T. N. Jones, "Radiation Effects on Pressure Vessel Steels," Radiation Metallurgy Section Solid State Division Progress Report for Period Ending July, 1966, ORNL-4020, 1, (1966).

²⁹R. G. Berggren, W. J. Stelzman, and T. N. Jones, "Radiation Effects on Pressure Vessel Steels," Radiation Metallurgy Section Solid State Division Progress Report for Period Ending July, 1967, ORNL-4195, 4, (1967).

³⁰N. E. Hinkle, N. K. Smith, and M. S. Wechsler, "Tensile Tests on Irradiated Iron," Radiation Metallurgy Section Solid State Division Progress Report for Period Ending Feb. 1966, ORNL-3494, 22, (1966).

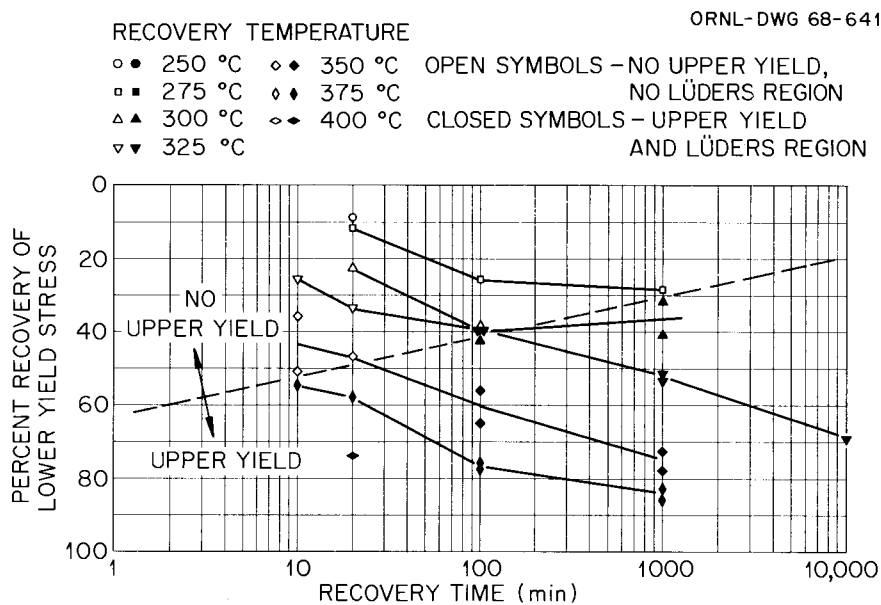


Fig. 11. Recovery of Yield Stress in Irradiated ASTM A-212-B Steel (1×10^{19} n/cm², $E > 1$ Mev, 60°C). SSD Item 157.

During the annealing studies, we observed consistent changes in the shape of the stress-strain curves of this irradiated steel. Specimens tested in the as-irradiated condition exhibited an upper yield point and a Lüders extension. The upper yield point was rounded as often observed in irradiated steels. After post-irradiation anneals at time-temperature combinations lying above the dashed line in Fig. 11, no upper yield point or Lüders extension were observed. The activation energy for this annealing range was about 1.0 to 1.5 ev. After post-irradiation anneals at higher temperatures and/or longer times (combinations lying below the dashed line of Fig. 11) the upper yield point and Lüders extension were observed and were very similar to the behavior of the unirradiated steel. The activation energy for this annealing range was about 2.5 to 3.5 ev. This change in yielding behavior is illustrated in Fig. 12 for 100 minute annealing times at the indicated temperatures.

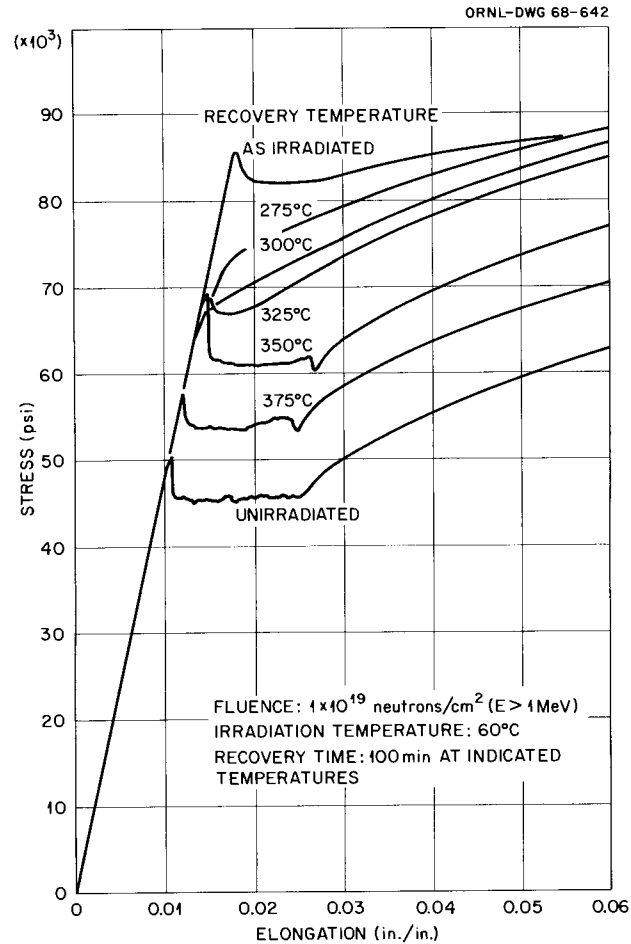


Fig. 12. Recovery Behavior of Irradiated ASTM A-212-B Steel (SSD Item 157).

The following qualitative interpretation emerges. The irradiation temperature was sufficiently high (50°C) for interstitial solutes to be mobile and therefore be trapped at radiation-produced defect clusters. In this condition the defect clusters give rise to a modified, somewhat weakened, yield point effect, as observed for the as-irradiated steel. Upon low temperature annealing (e.g. 275°C for 100 minutes), the trapped interstitial solutes dissociate from the defect clusters, the defect clusters may begin to anneal out, and very small nitride or carbide particles are formed, which do not contribute to a yield point phenomenon.

Finally, in the longer-time, high-temperature region (e.g. 350°C for 100 minutes) the smaller particles are dissolved, the interstitials return to solid solution, and the normal upper yield point and Lüders extension return.

Strain Aging of Neutron Irradiated Steel

W. J. Stelzman, R. G. Berggren, and J. T. Stanley

The term "strain aging" applies to processes which occur upon aging following plastic deformation, chiefly the gradual return of the upper yield point and Lüders strain and the increase in flow stress. The articles by Wilson and Russell^{31,32} provide a description of the phenomena as well as a number of references to other work. Various workers in this field are in general agreement that strain aging in steel is produced by the segregation of interstitial impurities such as carbon and nitrogen to dislocations where they form atmospheres or precipitates and thus prevent dislocation motion. Wilson and Russell and also others conclude that for a commercial steel slow cooled and tempered at 200°C for 2000 min., the strain aging effects are caused by nitrogen since carbon atoms are all precipitated as stable carbides. Strain aging also increases the ductile-brittle transition temperature of steel, and it has been determined that the effects of strain aging and neutron irradiation are additive in increasing the ductile-brittle transition temperature.³³

³¹D. V. Wilson and B. Russell, "The Contribution of Atmosphere Locking to the Strain-Aging of Low Carbon Steels," Acta Met., 8, 36, (1960).

³²D. V. Wilson and B. Russell, "The Contribution of Precipitation to Strain Aging in Low Carbon Steels," Acta Met., 8, 468, (1960).

³³M. Grounes and H. P. Myers, "Irradiation Effects in Strain-Aged Pressure Vessel Steel," Nature, 193, 468, (1962).

The interaction of interstitial impurities with radiation-produced defects undoubtedly influences the mechanical properties of irradiated iron and steel. There have been several studies^{34,35} using physical properties which show that both carbon and nitrogen interact strongly with radiation-produced defects, and there have been some studies which indicate that these interactions exert a profound influence on the mechanical properties.³⁶ These studies have been confined to relatively pure iron and their applicability to steel is somewhat indirect. The experiments described below constitute a preliminary investigation of the behavior of interstitial carbon or nitrogen in irradiated pressure vessel steel using the strain aging phenomena.

Experimental Procedures and Results

Specimens were strained in an Instron tensile machine located in a hot cell. The strain rate was $2.7 \times 10^{-4} \text{ sec}^{-1}$. Annealing was carried out in a vacuum furnace at a pressure of 10μ .

Figure 13b shows load-elongation curves for two specimens of ASTM A-212-B steel and illustrates the strain aging technique used in these experiments. The specimen given the strain aging treatment was pulled to a strain greater than the Lüders strain, unloaded, annealed at the temperature shown, and then re-strained. The effect of strain aging is apparent in Fig. 13 where the load-elongation curve of the strain

³⁴A. C. Damask, "Effect of Neutron Irradiation on Precipitation of Carbon in Alpha Iron," Diffusion in Body Centered Cubic Metals, 24, 317, ASM, Metals Park, Ohio, (1965).

³⁵M. Wuttig, J. T. Stanley, H. Birnbaum, "Interstitial Solute Trapping in Irradiated and Quenched Iron," submitted for publication.

³⁶N. E. Hinkle and N. K. Smith, "Tensile Tests on Irradiated Iron," Quarterly Progress Report: Irradiation Effects on Reactor Structural Materials, Nov., Dec. 1966-Jan. 1967, BNWL-CC-1053. Pacific Northwest Laboratory, Richland, Washington, 11.4-11.8, Feb. 15, (1967).

ORNL-DWG 68-666

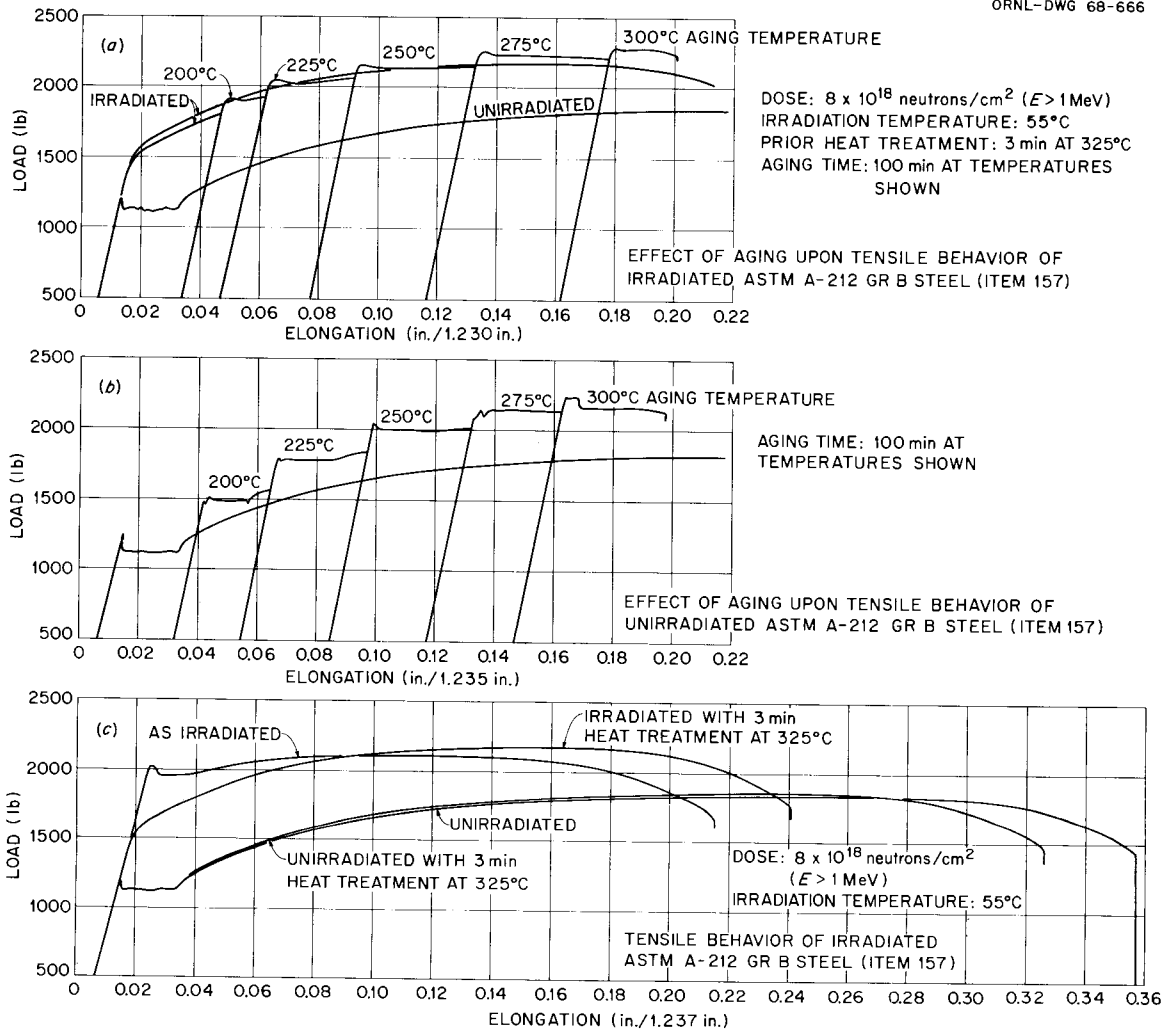


Fig. 13. Load-Elongation Curves for Unirradiated and Irradiated ASTM A-212-B Steel (Item 157).

aged specimen lies above that of the other specimen. It is convenient to define the strain aging effect by the quantity $\Delta\sigma = \sigma_{LY} - \sigma_f$, where σ_{LY} is the lower yield stress and σ_f is the flow stress observed in the preceding stress-strain cycle just before unloading. Wilson and Russell showed that restraining of a strain-aged specimen puts some of the nitrogen back into solution and allows the strain aging to reoccur.³² This mechanism accounts for the results observed in our experiments which were carried out with repeated strain aging cycles as shown in Fig. 13.

Figure 13a shows load-elongation curves for irradiated specimens of ASTM A-212-B steel and also the load-elongation curve for the unirradiated specimen shown in Fig. 13b. The results shown in Fig. 13a indicate that the strain aging effects are much smaller in the irradiated specimen compared to the unirradiated specimen.

The load elongation curves for unirradiated and irradiated specimens are compared in Fig. 13c with load elongation curves for both types of specimens given a three minute anneal at 325°C before testing. The effect of the 3 min anneal is negligible for the unirradiated specimen, but the load-elongation curve for the irradiated specimen is changed considerably.

The strain aging effect $\Delta\sigma$ is plotted vs aging temperature in Fig. 14 for the specimens discussed above and for some additional specimens. In the following discussion of Fig. 14 it is important to remember that the total strain increases as the temperature increases, and thus the changes shown in Fig. 14 may be partly a result of the preceding strain history of the specimen. Figure 14 shows results for two unirradiated specimens: an unirradiated specimen given no heat treatment other than that received during plate manufacture (open squares) and an unirradiated

specimen given an additional treatment of 10^4 min at 325°C (open circles). The results for this latter specimen are the most interesting because the strain aging anneals were started at a lower temperature than those for the former specimen. According to Wilson and Russell^{37,38} the maximum strain aging effect occurs in 10^4 min at 60°C . Assuming the strain aging effect is due to nitrogen, we calculate that 100 minutes at 150°C are equivalent to about 1100 minutes at 60°C , and 100 minutes at 200°C are equivalent to about 4×10^5 minutes at 60°C . Therefore, for the present experiment we would expect the maximum strain aging effect to occur between 150°C and 200°C , and this seems to agree with the results shown in Fig. 14 for the unirradiated specimen. The maximum strain aging effect observed by Wilson and Russell was 8000 psi³⁸ and this is in reasonable agreement with the present results. It seems likely that the decrease of strain aging effect with increasing temperature shown in Fig. 14 is more a function of strain history than increasing temperature.

The strain aging results for three irradiated specimens are also shown in Fig. 14. All of these irradiated specimens were given an anneal after irradiation and before testing. These results show that strain aging effects are greatly reduced by irradiation (filled triangles), presumably because the nitrogen is trapped and can no longer

³⁷D. V. Wilson and B. Russell, "The Contribution of Atmosphere Locking to the Strain-Aging of Low Carbon Steels," Acta Met., 8, 36, (1960).

³⁸D. V. Wilson and B. Russell, "The Contribution of Precipitation to Strain Aging in Low Carbon Steels," Acta Met., 8, 468, (1960).

migrate to the dislocations. However, upon annealing for 10^4 min at 325°C the traps for nitrogen are removed and the original strain aging effect is restored (filled squares). A short anneal (3 min at 325°C) restores only a fraction of the initial strain aging effect.

ORNL-DWG 68-906

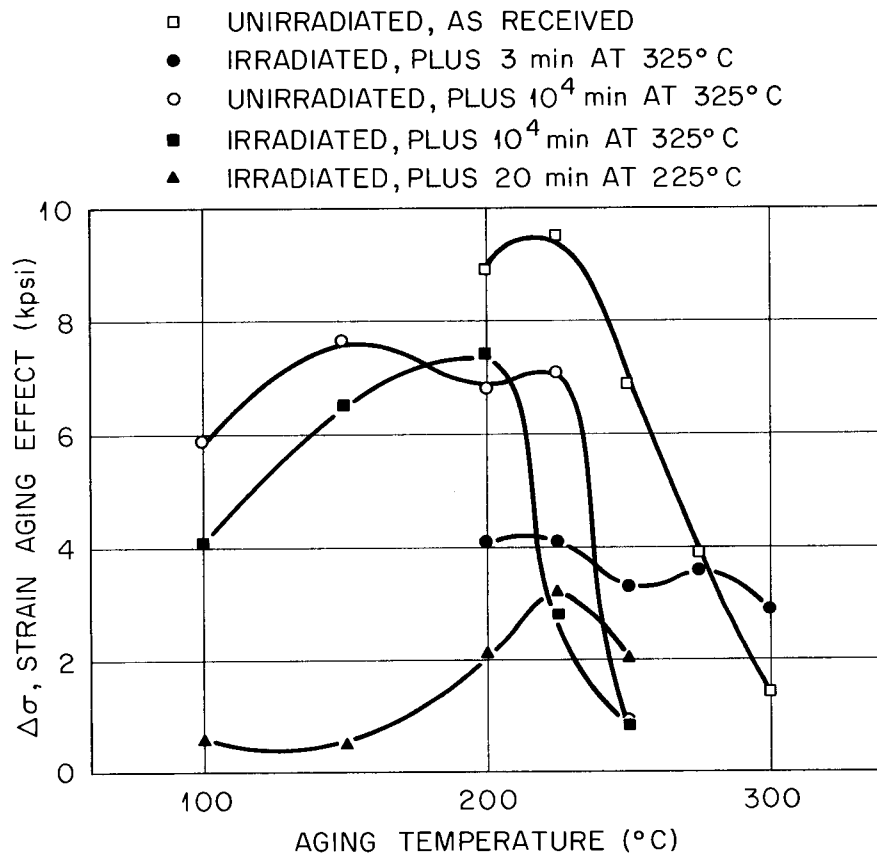


Fig. 14. Strain Aging of ASTM A-212 Gr. B. Steel (Item 157) as a Function of Aging Temperature. Aging Time 100 min. at Each Temperature Except 20 Minutes at Each Temperature for Triangle Points.

Effect of Thermal Neutrons on the Tensile Properties of ASTM A-212-B
and A-302-B Steels

R. G. Berggren, W. J. Stelzman, and M. S. Wechsler

Thermal neutrons can produce radiation damage in steels since the iron nucleus gains a significant recoil energy from the emission of gamma rays after capture of a thermal neutron.³⁹ We have previously reported⁴⁰ no observable difference in Charpy V-notch impact properties of unshielded and cadmium shielded specimens of ASTM A-212-B and ASTM A-302-B steels irradiated in the Oak Ridge Research Reactor. We have conducted tensile tests on specimens of these two steels irradiated in the same capsules as the previously reported Charpy V-notch specimens. Half of the specimens of each steel were irradiated inside a 0.040-inch-thick cadmium shield and the other specimens were irradiated without cadmium shielding. The results of these tension tests are presented in Table 3. No significant effect of cadmium shielding was observed in either steel. The tension tests were conducted at room temperature and a strain rate of 2.7×10^{-4} sec⁻¹. Exposure temperature was 60°C. In this irradiation facility a thermal to epithermal neutron ratio of 3:1 (cadmium ratio of 4:1) and a thermal to fast ($E > 1$ Mev) neutron ratio of 7.5:1 has been previously measured. A much higher thermal to fast neutron flux ratio will be required for study of the effects of thermal neutron irradiation.

³⁹M. S. Wechsler, "Fundamental Aspects of Radiation Effects on Diffusion-Controlled Reactions in Alloys," in Radiation Effects on Metals and Neutron Dosimetry, ASTM-STP-341, 86, American Society for Testing and Materials, Philadelphia, (1963).

⁴⁰R. G. Berggren, W. J. Stelzman, and T. N. Jones, "Radiation Effects on Pressure Vessel Steels," Radiation Metallurgy Section Solid State Division Progress Report for Period Ending July, 1967, ORNL-4195, 4, (1967).

Table 3. Tensile Properties of Irradiated ASTM A-212-B (SSD Item 157) and ASTM A-302-B (SSD Item 127-D) Steels and Effect of Cadmium Shielding

SSD Item	Fast Neutron Dose (E > 1 Mev)	Irradiation Temperature (°C)	Upper Yield (ksi)	Lower Yield (ksi)	Ultimate Strength (ksi)	Fracture Strength (ksi) ^(a)	Elongation		
							Luders (%)	Uniform ^(b) (%)	Total ^(c) (%)
	(x 10 ¹⁸ n/cm ²)								
157(e)	0	--	--	44.7	74.1	58.7	1.5	18.3	27.7
	0	--	--	44.2	74.1	58.3	--	--	--
	0	--	--	45.2	74.4	59.3	1.7	19.1	29.9
	0	--	--	44.6	74.1	58.3	1.6	18.2	27.8
Without Shielding	4.5	70	76.6	75.2	82.9	65.4	1.9	10.7	18.8
	5.1	70	79.3	77.3	84.1	67.5	2.1	9.3	17.1
Cadmium Shielded (d)	4.5	70	77.0	74.6	83.1	65.7	1.7	11.5	21.7
	5.1	72	78.1	76.3	82.8	64.8	2.0	10.8	20.0
	5.5	73	78.6	77.2	84.3	67.5	1.5	8.2	17.8
127-D (e)	0	--	57.0	56.6	84.5	63.8	0.8	12.9	20.9
	0	--	--	54.5	82.7	58.9	0.9	12.7	21.1
	0	--	--	54.9	82.7	62.2	0.7	14.6	23.4
	0	--	57.3	55.3	83.6	62.7	0.8	11.5	18.7
Without Shielding	4.8	64	91.5	88.2	92.9	66.0	2.8	5.8	13.7
	5.5	67	92.9	89.9	93.3	68.5	0.5	5.7	13.5
	5.8	69	94.1	91.5	94.3	68.4	1.2	4.9	12.7
Cadmium Shielded (d)	5.1	67	92.7	89.3	93.7	71.1	3.1	7.1	15.5
	5.5	71	93.9	90.5	93.9	69.0	1.8	6.1	14.3
	5.5	73	92.7	90.5	93.7	68.8	2.3	5.4	12.3

^aFracture load/original area

^bAverage elongation at maximum load

^cFrom load-elongation record

^dSpecimen shielded with 0.040 inches cadmium

^eItem 157 from 1/4 thickness; Item 127-D from 1/3 thickness

Properties of 12-Inch-Thick ASTM A-533-B, Class I, Steel*

R. G. Berggren and T. N. Jones

Material characterization tests are in progress on the first 12-inch-thick plate of ASTM A-533-B, Class I, steel procured for the Heavy Section Steel Technology (HSST) program. This steel was formerly known as ASTM A-302-B, modified (per ASME Pressure Vessel Code, Interpretation Case 1339). Material from this plate will be incorporated in our irradiation effects studies when characterization tests indicate this plate is satisfactory for irradiation studies. Characterization tests will include tensile tests, Charpy V-notch impact tests, Drop weight tests (P-1, P-2, and P-3 specimens), hardness, chemical composition, and metallographic examination. Tests are being conducted on longitudinal, transverse, and through-thickness specimens cut from several depths in the plate.

This first 12-inch-thick ASTM A-533-B, Class I, plate (HSST plate 01) was produced by the Lukens Steel Company. The ingot (138,000 pounds) was produced in a basic electric furnace, aluminum deoxidized (0.7 lb/ton), and vacuum degassed in the ladle. The ingot was 108 inches wide, 40 inches thick, and 127 inches high. The ingot was then slabbed and rolled to plate form. The rolling reduction ratio was 3.33, cross rolling ratio 1.4, and the finishing temperature was 1650°F. The plate was sand cooled after rolling. The trimmed plate weighed 106,420 pounds and measured 260 inches long, 120 inches wide, and 12 inches thick. The mill test report is given in Table 4.

*Work conducted under the Heavy Section Steel Technology Program.

The plate was heat treated by Combustion Engineering, Inc. Heat treatment consisted of normalizing (1675-1700°F for 4 hours and air cooling) to simulate hot-forming operations, austenitizing at 1550-1650°F for 4 hours, quenching in agitated water, tempering at 1225°F for 4 hours, and air cooling. The plate was then flame cut and stress relieved at 1125-1175°F for 40 hours. All heat treatment operations were monitored with thermocouples buried in the plate.

Test results, already obtained for specimens from the central region of this plate, are presented in Fig. 15. As expected, the highest yield and ultimate strengths and the lowest Drop Weight NDT temperatures were obtained for specimens from near the plate surfaces. The properties are quite uniform through the central eight inches of the plate except for some decrease in ductility and hardness at the mid-thickness. The slightly poorer properties at mid-thickness are probably due to the higher inclusion content observed at mid-thickness.

Table 4. Mill Test Report for HSST Plate 01, ASTM
A-533 Grade B, Class I Steel, Lukens Heat No. A1008.

<u>Chemical Composition</u>	<u>Ladle</u>	<u>Check</u>
Carbon	0.22%	0.22%
Manganese	1.45%	1.48%
Phosphorus	0.011%	0.012%
Sulfur	0.019%	0.018%
Silicon	0.22%	0.25%
Nickel	0.62%	0.68%
Molybdenum	0.53%	0.52%

Physical Properties:

Yield Strength	70,100 psi
Ultimate Tensile Strength	95,000 psi
	93,600 psi
Elongation (2")	27%

Test pieces heated to 1575-1625°F, held 4 hours, program cooled per cooling rate for 12 inch plate, tempered at 1200-1250°F held 4 hours and cooled, then stress relieved at 1125-1175°F held 20 hours and furnace cooled to 600°F.

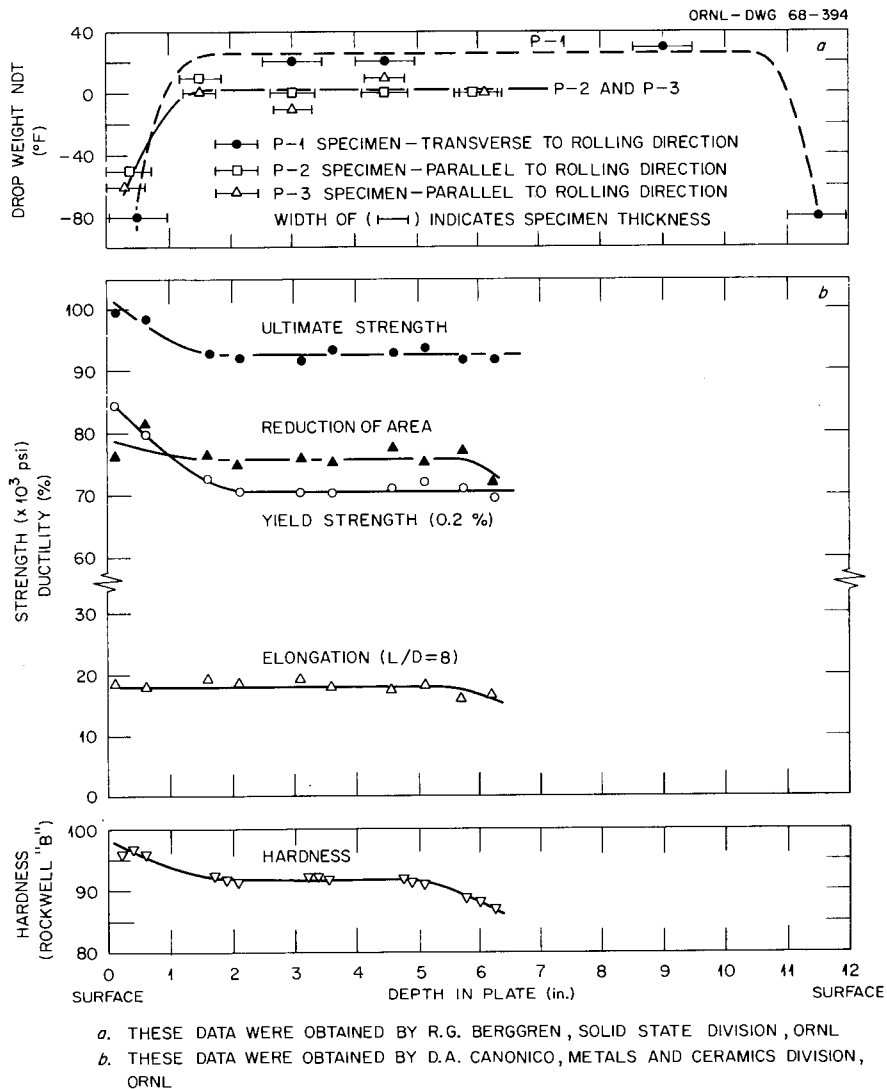


Fig. 15. Mechanical Properties of HSST Plate 01; 12-Inch Thick ASTM A-533-B, Class I Steel (Central Region).

The Interaction Between Oxygen and Radiation-Produced Defects in Niobium

J. T. Stanley, J. M. Williams, and W. E. Brundage

Introduction

In previous reports^{41-43,44} we have shown that oxygen migrates to radiation-produced defects in neutron-irradiated niobium upon annealing at temperatures near 150°C. A kinetic analysis has been presented⁴⁵ which supports the hypothesis that small dislocation loops act as traps for the oxygen atoms. In the present report, results are presented which show that oxygen trapped at the dislocation loops can be returned to solution by annealing above 250°C.

Experimental Procedures

The work described in this report was carried out on specimens described previously⁴³. Briefly, several specimens were prepared containing 50 ppm oxygen and irradiated to a fluence of 2×10^{18} neutrons,

⁴¹J. T. Stanley and W. E. Brundage, "The Interaction of Radiation Produced Defects and Interstitial Impurity Atoms in Niobium," Quarterly Progress Report: Irradiation Effects on Reactor Structural Materials, May-June 1966, BNWL-CC-784. Pacific Northwest Laboratory, Richland, Washington, 10.30, August (1966).

⁴²J. M. Williams, J. T. Stanley, and W. E. Brundage, "The Interaction of Radiation Produced Defects and Interstitial Impurity Atoms in Niobium," Quarterly Progress Report: Irradiation Effects on Reactor Structural Materials, Nov. 1966-Jan. 1967, BNWL-CC-1053. Pacific Northwest Laboratory, Richland, Washington, 11.18, February (1967).

⁴³J. T. Stanley, J. M. Williams, W. E. Brundage, "The Effect of Oxygen on 'Stage III' Annealing in Neutron-Irradiated Niobium," Quarterly Progress Report: Irradiation Effects on Reactor Structural Materials, May-July 1967, BNWL-532. Pacific Northwest Laboratory, Richland, Washington, 11.17, August (1967).

⁴⁴J. M. Williams, W. E. Brundage, and J. T. Stanley, "The Effect of Oxygen on 'Stage III' Annealing in Neutron-Irradiated Niobium," to be published in *Metals Science Journal*.

⁴⁵R. Bullough, J. T. Stanley, and J. M. Williams, "The Kinetics of Migration of Impurities to Small Dislocation Loops," to be published in *Metal Science Journal*.

$E > 1$ MeV, at 50°C . The specimens were placed in the torsion pendulum apparatus and annealed at approximately 150°C for about 10^4 minutes. Internal friction measurements were made at frequent intervals during this anneal period. After this initial anneal period, internal friction measurements were made as a function of temperature and the results will be described below.

In some instances the specimen was removed from the torsion pendulum, annealed in a high vacuum furnace, and then replaced in the torsion pendulum for further measurements. The high-vacuum system used in these anneals employed a liquid-nitrogen cold trap and metal gasket seals. A pressure of about 1×10^{-7} torr was maintained during the anneal. The specimen was placed in a fused quartz tube attached to this system and heated by an external furnace. It was not possible to achieve rapid heating or cooling in this system. One specimen was annealed in situ in the torsion pendulum. In this case somewhat more rapid heating and cooling was obtained, but the vacuum was not as good (about 5×10^{-5} torr) and the specimen was stressed (about 4000 psi) during the anneal.

Results

The migration of oxygen to radiation-produced traps and thus its effective removal from solid solution can be detected independently by internal friction and electrical resistivity measurements. In the previous work,⁴³ a rather close agreement in the fractional decrease of the two properties upon post-irradiation annealing at 150°C was shown, although some discrepancy existed toward the mid-range of the annealing (see Fig. 10, Ref. 43). A second niobium sample cut from the same wire

and given an identical thermal and irradiation treatment as the previous sample has now been tested. Using improved temperature measurement and control for the internal friction measurements, we find that the resistivity and internal friction results agree over the entire annealing range (Fig. 16).

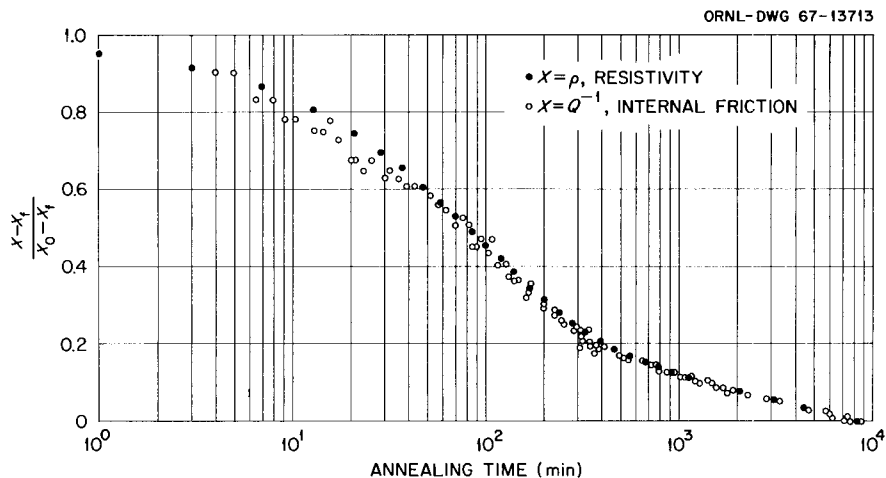


Fig. 16. Normalized Resistivity and Internal Friction Decrease Versus Log of Annealing Time at 150°C for Sample G-3 (Resistivity) and G-2 (Internal Friction) Irradiated to 2×10^{18} n/cm² ($E > 1$ Mev) at 40-50°C. X_0 and X_f Refer to the Property Immediately After Irradiation and After Annealing for 8000 min., respectively.

The close comparison between the annealing kinetics of resistivity and internal friction is significant because it bears on the origin of the "Stage III" post-irradiation resistivity annealing observed at about $0.15 T_m$ (T_m = melting temperature) for the BCC metals generally. The internal friction peak at 150°C in niobium is known to be due to oxygen in solid solution, and thus the "Stage III" resistivity decrease in niobium must also be due to oxygen. By inference, we are led to suspect that the "Stage III" annealing in the other BCC metals is also due to interstitial impurities.

Since the oxygen is now known to be removed from solid solution at radiation-produced defect traps, the question arises as to how high a temperature is necessary to dissociate the oxygen from the defect traps. Figure 17 shows internal friction as a function of temperature of measurement up to 340°C for a sample previously irradiated and then annealed (aged) at 150°C for about 10^4 minutes. Two broad peaks, centered at 230 and 270°C are seen in addition to the residual oxygen peak at 160°C . These additional peaks are no longer present after the first run (circles), as can be seen from the second run (triangles). Figure 17 also shows that the 150°C oxygen peak is increased for the second run; this is discussed further below.

Figure 18 shows internal friction measurements made on another irradiated specimen after the 150°C aging. The measurements again indicate the presence of additional internal friction peaks at temperatures above the oxygen peak, but in this case the measurements were interrupted starting at 250°C to return to the oxygen peak temperature (153°C). Upon returning to the higher temperatures, a decrease in the internal friction was noted at 240°C , at 250°C , and at 260°C . Then the measuring temperature was reduced to 153°C for another measurement of the oxygen peak height. Upon returning again to 250°C , a further decrease in the internal friction was noted. Thus, the high temperature peaks were removed by temperature cycling. Figure 18 also shows the internal friction measurements after annealing at 300°C (triangles) and over a range from 325° to 400°C (filled circles). After annealing at these temperatures, the oxygen has returned to solution. The background internal friction at temperatures above the oxygen peak is

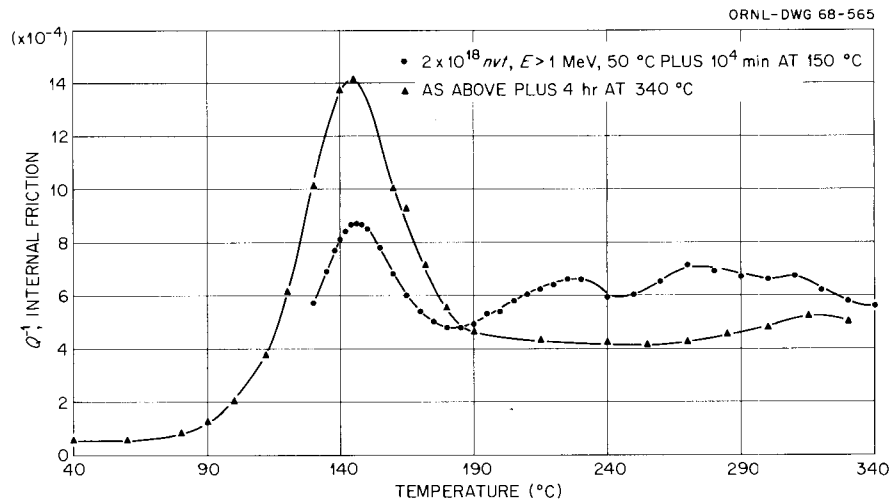


Fig. 17. Internal Friction of Neutron-Irradiated Niobium Containing 50 ppm Oxygen. Frequency = 0.9 cps. Sample G-1.

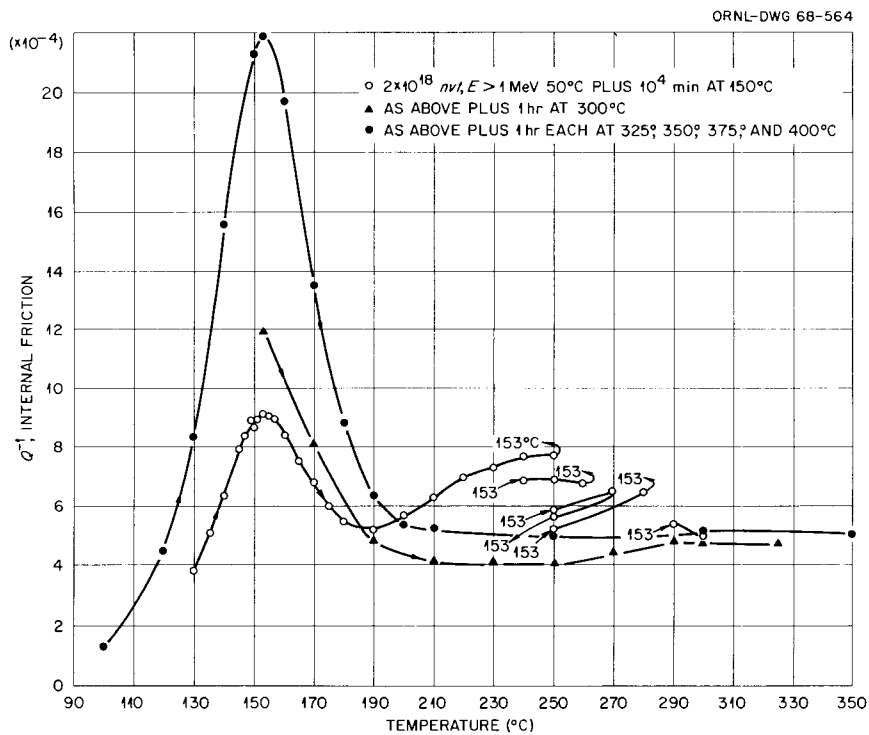


Fig. 18. Internal Friction of Neutron-Irradiated Niobium Containing 50 ppm Oxygen. Frequency = 1.37 cps. Sample G-2.

higher than at temperatures below the oxygen peak. The same feature occurs in the unirradiated specimen but is not so large.

In Fig. 19 the height of the oxygen peak is plotted as a function of annealing temperature for the two irradiated specimens discussed above. Note that the oxygen peak returns at lower annealing temperatures for the stressed specimen even though the annealing time is shorter. Also for anneals at 350°C or lower the oxygen peak shows a slight decrease upon additional aging at 150°C. The oxygen peak height is greater than before irradiation for specimen G-1 annealed at 500°C for 4 hours, and the shape of the curve for specimen G-2 suggests that it will also go above the original peak height after additional anneals at a higher temperature. The measurement of the oxygen peak height of specimen G-1 after the 500°C anneal was made twice. First the peak height was measured on the specimen as annealed, and then the specimen was removed from the torsion pendulum and etched to remove about 0.002 in. from its diameter. After this latter treatment the peak height was again measured and found to be the same as the peak height before etching. Thus the increase of the oxygen peak above the pre-irradiation value is not due to surface contamination by pick-up of oxygen from the vacuum system during annealing.

Discussion

The internal friction measurements described above have shown several new features which must be explained by any model of the trapping mechanism:

- (1) Two new internal friction peaks appear in irradiated niobium containing oxygen;
- (2) These new peaks are removed by cycling between high and low temperatures;
- (3) The background internal friction at temper-

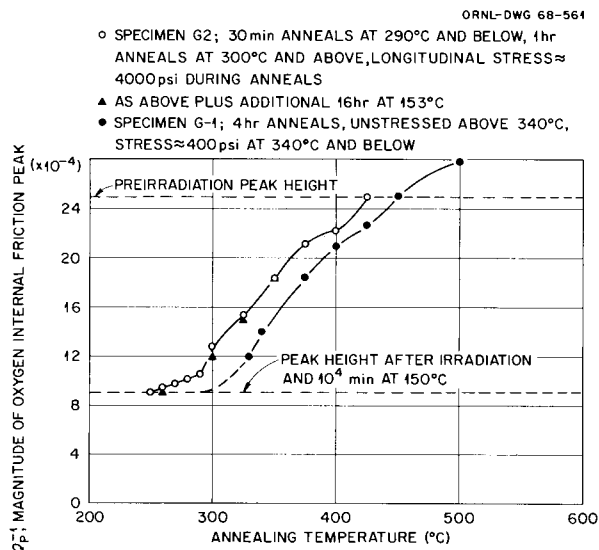


Fig. 19. The Return of Oxygen to Solution in Irradiated Niobium. Specimens G-1 and G-2 Irradiated to 2×10^{18} n/cm² ($E > 1$ Mev) at 40-50°C and Annealed $\approx 10^4$ minutes at $\approx 150^\circ\text{C}$, then Annealed at Temperatures and Times Shown.

atures above the oxygen peak is increased by irradiation; (4) The traps for the oxygen anneal out when the oxygen dissociates from them; (5) A uniaxial stress applied during the anneal aids in removal of the traps; (6) After irradiation and annealing to about 500°C, the oxygen peak is higher than before irradiation. Possibly all of these points are not directly connected with the trapping mechanism, and in particular, feature 6 might be observed in unirradiated specimens. We have postulated that the small dislocation loops produced by irradiation act as traps for the oxygen atoms, and we believe that all of the above features can be explained by this mechanism.

In particular, the extra peaks may be analogues of the cold work peak observed in deformed b.c.c. metals which contain interstitial impurities. These cold work peaks have been the subject of a number of

investigations,⁴⁶⁻⁵⁰ and several different models have been proposed to account for the observations. In Schoeck's⁵¹ model of the cold work peak the anelastic strain arises from motion of the dislocation, which is restricted by the drag of the impurity atmosphere. According to this model the peak temperature depends on the length of the dislocation segment between nodes or precipitate pinning points. This feature would explain the lower temperature of the peaks in the neutron-irradiated specimen (-230°C and 270°C) compared to the temperature of the oxygen cold work peak in niobium which is at about 420°C.⁵⁰ The same effect would also explain the presence of two peaks in neutron-irradiated niobium if we assume two distinct loop sizes, one size for vacancy loops and another for interstitial loops. However, more experiments must be performed before a detailed theory can be developed. The peculiar way in which these peaks disappear upon thermal cycling is somewhat difficult to explain. One possibility is that precipitation of an

⁴⁶W. Köster, L. Bangert, and R. Hahn, "Das Dämpfungsverhalten von gerecktem technischem Eisen," *Archive Eisenhüttenw.*, 25, 569, (1954).

⁴⁷K. Kamber, D. Keefer, and C. Wert, "Interactions of Interstitials with Dislocations in Iron," *Acta Met.*, 9, 403, (1961).

⁴⁸D. P. Petarra, "Internal Friction in Iron at Temperatures in the Range 0°C to 500°C at Frequencies near 1 c/s," Thesis, Columbia University (New York, 1962).

⁴⁹G. Schoeck and M. Mondino, "Internal Friction Due to Interstitial-Dislocation Interaction in Ta," *J. Phys. Soc. of Japan*, 18, Suppl. 1, 149, (1963).

⁵⁰D. J. van Ooijen and A. S. van der Goot, "The Internal Friction of Cold-Worked Niobium and Tantalum Containing Oxygen and Nitrogen," *Acta Met.*, 14, 1008, (1966).

⁵¹G. Schoeck, "Friccion Interna Debido a La Interaccion Entre Dislocaciones Y Atomos Solutos," *Acta Met.*, 11, 617, (1963).

oxide takes place on the dislocation loop. The precipitates do not form at the higher temperature because of a low supersaturation factor, but upon cooling to low temperature nucleation takes place. The increase of background internal friction at temperatures above the Snoek peak is also observed in cold worked material, but no detailed explanation for this effect has been given.

The conclusion that dissociation of oxygen from the traps and annealing of the traps occur simultaneously (point 4 above) is drawn from the observation that the peak height observed immediately after a high temperature anneal is not changed substantially by an additional aging treatment of up to 16 hours at 153°C. Figure 16 shows that 16 hours (960 minutes) is long enough to complete most of the trapping reaction in the as-irradiated specimen. It is true that for anneals at or below 325°C there was some slight amount of retrapping of oxygen after the 16-hour aging at 153°C. This behavior would be expected from the nature of the dislocation traps. A calculation shows that about 7 oxygen atoms are trapped for each lattice point on the dislocation core. It is likely that all of the oxygen atoms which are trapped are not in the dislocation core. Thus, we would expect the oxygen atoms which are at the edge of the atmosphere to be rather loosely bound. These loosely bound atoms might evaporate at moderately elevated temperatures leaving the dislocation core still filled with tightly bound atoms. It is only after these tightly bound oxygen atoms have evaporated that the dislocation loop can anneal out. This mechanism suggests that annealing of loops in specimens containing other interstitial impurities such as carbon or nitrogen might occur at a different temperature than in a specimen containing only oxygen.

The effect of stress in aiding the annealing process is a rather unexpected result. We believe that the stress of 4000 psi is below the yield stress of this specimen at the temperature of the measurement. The specimen was examined in the microscope after the measurements were made, and no visible signs of flow were seen. An upper limit of 1.6% elongation can be set on the strain since the difference of specimen length before and after the measurements was known to be less than 1/16 inch.

The increase of peak height above the value observed before irradiation (point 6) indicates that some of the oxygen was trapped at a defect structure before the irradiation. It is possible that vacancy loops or clusters formed during the cooling of the specimen from the final annealing temperature (1100°C) prior to irradiation and that part of the oxygen became trapped at these defects.

Trapping of Oxygen and Nitrogen in Neutron-Irradiated Vanadium

J. T. Stanley, J. M. Williams, and W. E. Brundage

Several years ago we attempted to observe the trapping of oxygen and nitrogen in neutron-irradiated vanadium. Only a small decrease in the oxygen and nitrogen peaks was observed after a neutron fluence of 5×10^{17} neutrons/cm², $E > 1$ Mev.⁵² We have now irradiated additional vanadium specimens to a higher fluence, 7.2×10^{17} $E > 1$ Mev, and measured the decrease of the oxygen and nitrogen peaks as a function of time at the peak temperatures.

⁵²J. T. Stanley, "In-Reactor Internal Friction Measurements of Interstitial Rearrangements in BCC Metals," Quarterly Progress Report: Irradiation Effects on Reactor Structural Materials, Nov., Dec., 1963 and Jan., 1964, HW-80794, Hanford Laboratories, Richland, Washington, 10.1, February (1964).

Figure 20 shows the internal friction as a function of temperature for one of the unirradiated specimens. The oxygen peak at 182°C is considerably wider than would be expected for a single relaxation process, and we believe that this specimen may also contain carbon. According to Powers and Doyle⁵³ the carbon peak occurs at 170°C while the oxygen peak occurs at 182°C in vanadium for 1 cps vibration frequency.

Figure 21 shows the relative decrease of the oxygen and nitrogen peaks as a function of time at the respective peak temperatures, 185°C and 275°C respectively. For these measurements the specimen was held first at the oxygen peak temperature (185°C) and the oxygen peak decreased to about 50% of its initial value. The specimen was then held at the nitrogen peak temperature (275°C), and the nitrogen peak decreased to about 80% of its initial value. Upon returning to the oxygen peak temperature some recovery of the oxygen peak was noted.

The total amount of nitrogen in solution before irradiation was about 1200 ppm atomic while the amount of oxygen in solution was only 167 ppm, as determined by the internal friction peak heights and conversion factors given by Powers and Doyle.⁵³ Thus the fact that some of the oxygen is apparently forced out of the loops by the nitrogen does not necessarily mean that the binding energy of nitrogen atoms to dislocations is greater than that of oxygen, since nitrogen is present in much greater amounts than oxygen.

⁵³R. W. Powers and M. V. Doyle, "Diffusion of Interstitial Solutes in Group V Transition Metals," J. Appl. Phys., 30, 514, (1959).

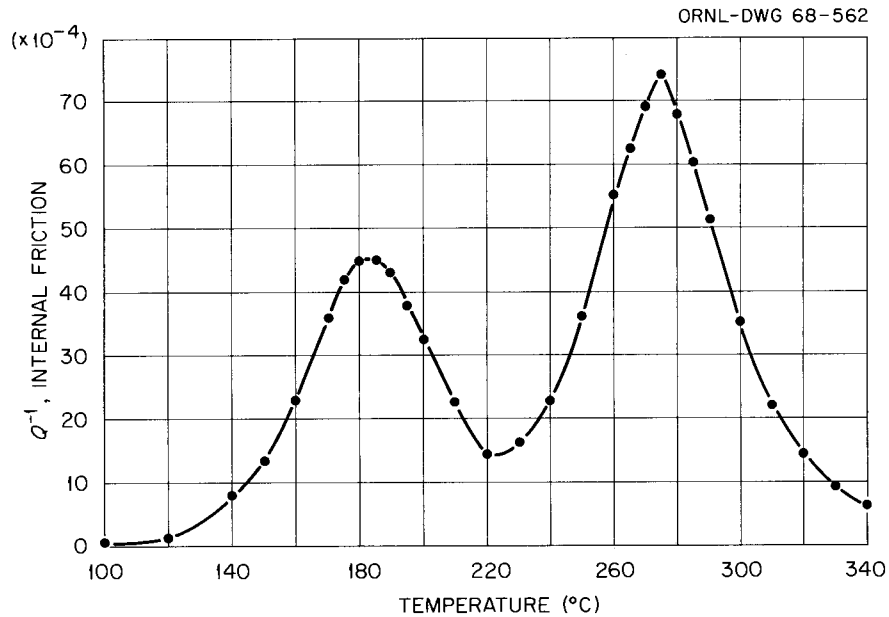


Fig. 20. Internal Friction of Vanadium as a Function of Temperature, Specimen V-D-3 Annealed 45 min. at $\approx 230^\circ\text{C}$, 3×10^{-8} torr. Frequency 1.12 cps.

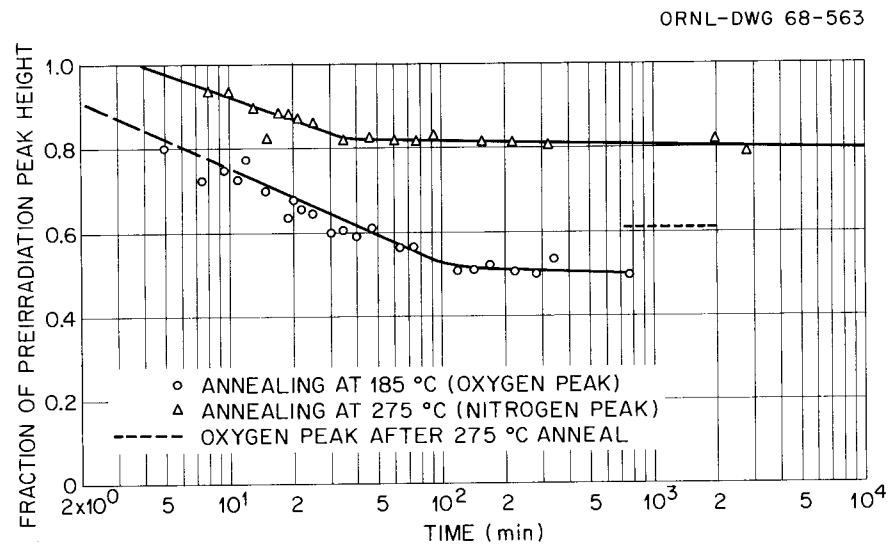


Fig. 21. Relative Decrease With Time of Oxygen and Nitrogen Peaks of Neutron-Irradiated Vanadium Specimen V-D-3. Fluence 7×10^{17} n/cm² ($E > 1$ Mev) at 60°C .

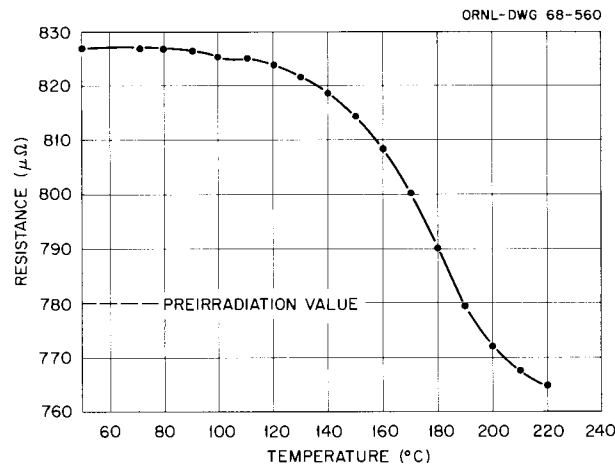


Fig. 22. Isochronal Annealing of Resistance of Vanadium Specimen V-D-5 Neutron-Irradiated to 7×10^{17} n/cm² ($E > 1$ Mev) at 60°C. Annealing Time 20 min. at Each Temperature Shown.

Figure 22 shows the resistivity decrease of a neutron-irradiated vanadium specimen as a function of annealing temperature. This specimen contained the same amount of interstitial impurity as the internal friction specimen discussed above, and was given an identical irradiation. As the figure shows, there is a large resistivity annealing stage centered at about 180°C, which corresponds with the temperature of the oxygen internal friction peak. Presumably another resistivity annealing stage corresponding to the nitrogen internal friction peak will be observed as the annealing temperature is increased further. It was mentioned above that the internal friction measurements indicated the presence of carbon in solution in this specimen in addition to oxygen and nitrogen. Since the carbon and oxygen atoms have very nearly equal jump rates at a given temperature, we would expect the resistivity annealing stages for carbon and oxygen to overlap. There is a small dip in the resistivity annealing curve shown in Fig. 22 at 100°C, which could be caused by the slightly greater mobility of carbon. This dip

does not show up very well in the figure because of the scale, but it is certainly a real effect and very apparent when the data are plotted on an expanded scale. The annealing stage shown in Fig. 22 occurs at a homologous temperature of about $0.21 T_m$. The $0.15 T_m$ temperature for vanadium is 50°C .

The Annealing Characteristics of Neutron Irradiated Niobium

S. M. Ohr, R. P. Tucker,* and E. D. Bolling

Sometime ago, Makin and Minter⁵⁴ first reported the observation of a large increase in the yield stress in neutron irradiated niobium upon post-irradiation annealing. They concluded that in their niobium "radiation-anneal hardening" resulted from the condensation of radiation-produced vacancies along dislocation lines. In a recent study using internal friction and electrical resistivity techniques, Williams *et al.*⁵⁵ found that the temperature range and activation energy associated with the previously reported radiation-anneal hardening agree closely with those characteristic of oxygen migration in niobium. Support for attributing the hardening to oxygen lies in the high oxygen impurity level of 1600 wt ppm reported by Makin and Minter.

In the present study, the annealing characteristics of neutron irradiated niobium, relatively free of oxygen, have been investigated in

*Oak Ridge Graduate Fellow from the University of Tennessee under appointment from Oak Ridge Associated Universities.

⁵⁴M. J. Makin and F. J. Minter, "The Mechanical Properties of Irradiated Niobium," *Acta Met.*, 7, 361, (1959).

⁵⁵J. M. Williams, J. T. Stanley, and W. E. Brundage, "The Interaction of Radiation Produced Defects and Interstitial Impurity Atoms in Niobium," Quarterly Progress Report: Irradiation Effects on Reactor Structural Materials, Nov. 1966-Jan. 1967, BNWL-CC-1053. Pacific Northwest Laboratory, Richland, Washington, 11.18, February (1967).

terms of tensile properties and transmission electron microscopy. Using the electron microscope, direct observations have been made of the annealing of irradiation induced defects. In particular, the defect size distribution following post-irradiation anneals was measured in order to seek microstructural evidence for the radiation-anneal hardening observed for annealing temperatures of 200°C and higher. Also, the nature of the defects has been investigated.

Experimental Procedures

The niobium used in this study was obtained from the CIBA Corporation in the form of dendritic powder. Thin sheet tensile samples of 0.005-inch thickness were prepared by cold rolling single crystal rods grown by an electron beam floating zone technique.⁵⁶ These sheet samples were given a recrystallization anneal at 1050°C for one hour in a dynamical vacuum of approximately 3×10^{-8} torr to give an average grain size of 44μ . The impurity content was determined at this point and the results are shown in Table 5. Irradiation was carried out in the Hydraulic Facility of the Oak Ridge Research Reactor to a fluence of 2×10^{18} neutrons/cm² ($E > 1$ Mev) at a temperature below 50°C.

Both irradiated and unirradiated samples were annealed for two hours at temperatures from 200°C to 800°C in a vacuum better than 10^{-8} torr. Thin foils suitable for transmission electron microscopy were prepared by electropolishing in a solution, 85 parts nitric acid and

⁵⁶R. E. Reed, "Electron Beam Floating Zone Refining of Niobium," in Proceedings of the Second International Conference on Electron and Ion Beam Science and Technology, April 17-20, 1966, Gordon and Breach Publishers, New York. To be published.

15 parts hydrofluoric acid by volume. The foils were examined in the Hitachi 11 A electron microscope operated at 100 kv and equipped with tilting and rotating stages.

Tensile Results

Figure 23 shows the lower yield stress, determined at 24°C, of irradiated and unirradiated samples as a function of annealing temperature for two hour anneals. In addition to an increase in the yield stress of 5.8 kg/mm² upon neutron irradiation, there is a further increase of up to 8.5 kg/mm² on annealing in the temperature range 200 to 400°C. As the annealing temperature is raised further the yield stress gradually recovers and finally reaches the pre-irradiation value at 800°C.

A characteristic feature of the present observations is radiation-anneal hardening in the temperature range 200 to 400°C; whereas, Makin and Minter observed hardening in the range 100 to 200°C. Furthermore, it should be emphasized that we observed no radiation-anneal hardening in the range 100 to 200°C even though the annealing time employed in the present study is two hours compared to one hour used by Makin and Minter. A second point of interest is the increase in the yield stress of unirradiated samples also in the range of 200 to 400°C.

In regard to the yielding characteristics we have noted that the yield drop, that is prominent after neutron irradiation, diminishes upon annealing up to the annealing temperature of 400°C. The yield drop then returns after anneals at temperatures greater than 500°C.

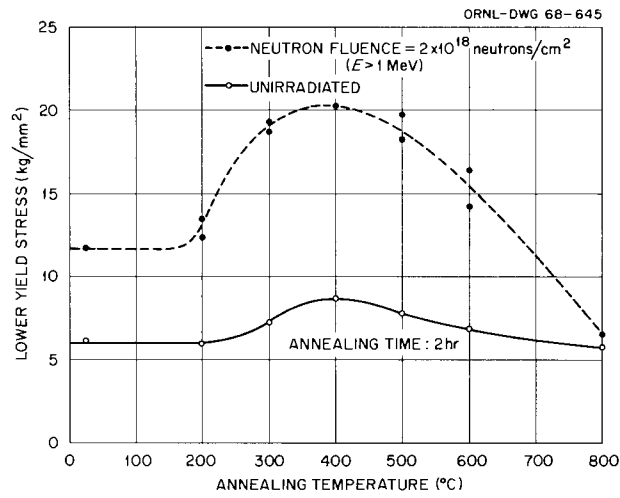


Fig. 23. The Lower Yield Stress of Neutron-Irradiated and Unirradiated Niobium as a Function of Annealing Temperature for Two-Hour Anneals.

Table 5

IMPURITY CONTENT OF NIOBIUM IN WEIGHT PARTS PER MILLION

<u>Impurity</u>	<u>Content</u>	<u>Impurity</u>	<u>Content</u>
C	60	Ta	20
O	38	W	10
H	2	Zr	10
N	5	Hf	5
		Fe	1

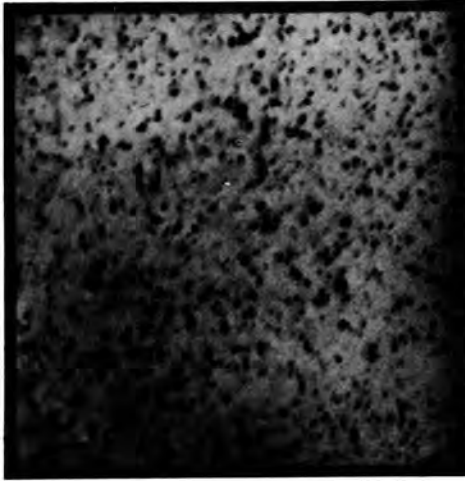
Transmission Electron Microscopy

Figure 24 shows irradiation damage in the form of black spots under the kinematical diffraction condition for samples irradiated and subsequently annealed for two hours at 200, 300, and 400°C. Plots of the defect density as a function of spot size, measured on a Zeiss particle size analyzer, for as-irradiated and after the post-irradiation anneal at 400°C are shown in Fig. 25. Although more counts are needed to assess accurately changes upon annealing, there is a significant change in the peak size from 80 Å to 130 Å. There is a very slight decrease in the overall density of spots, which indicates that the defects simply grow in size in this range of temperatures.

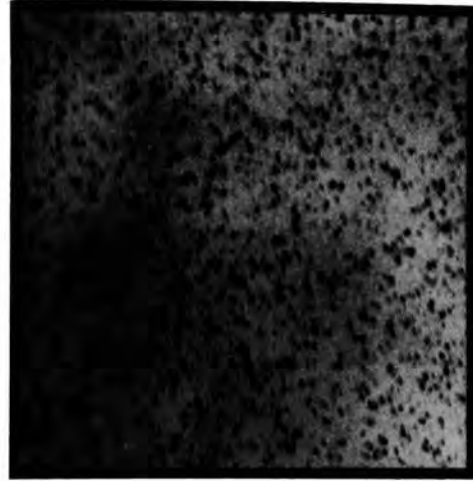
The annealing of defects after two hours at 500, 600, and 800°C is shown in Fig. 26. The most noticeable feature is the appearance of numerous small spots throughout the sample after the anneal at 600°C. Figure 27 shows that the usual large defects have been denuded in the vicinity of a grain boundary, whereas the small defects show no denudation at the grain boundary. These observations are similar to those made by Makin et al.⁵⁷ in neutron irradiated copper following a mild anneal at 300°C. They inferred that the large defects are formed by the condensation of interstitial atoms and the small defects are vacancy clusters.

⁵⁷M. J. Makin, A. D. Whapham, and F. J. Minter, "The Formation of Dislocation Loops in Copper During Neutron Irradiation," Phil. Mag., 7, 285, (1962).

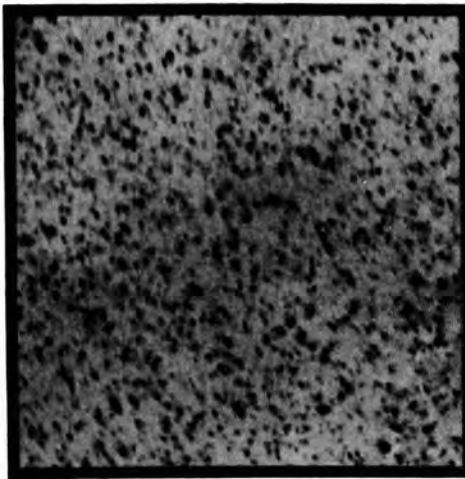
PHOTO 90504



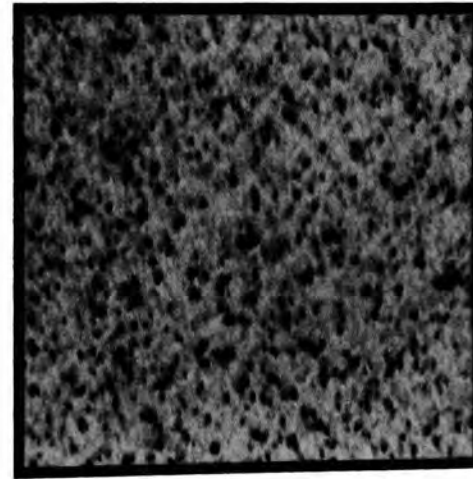
As-Irradiated



200°C

0.3 μ

300°C



400°C

Fig. 24. Spot Damage in Neutron-Irradiated Niobium After Two-Hour Post-Irradiation Anneals at Temperatures Indicated. Fluence, 2×10^{18} neutrons/cm², $E > 1$ Mev.

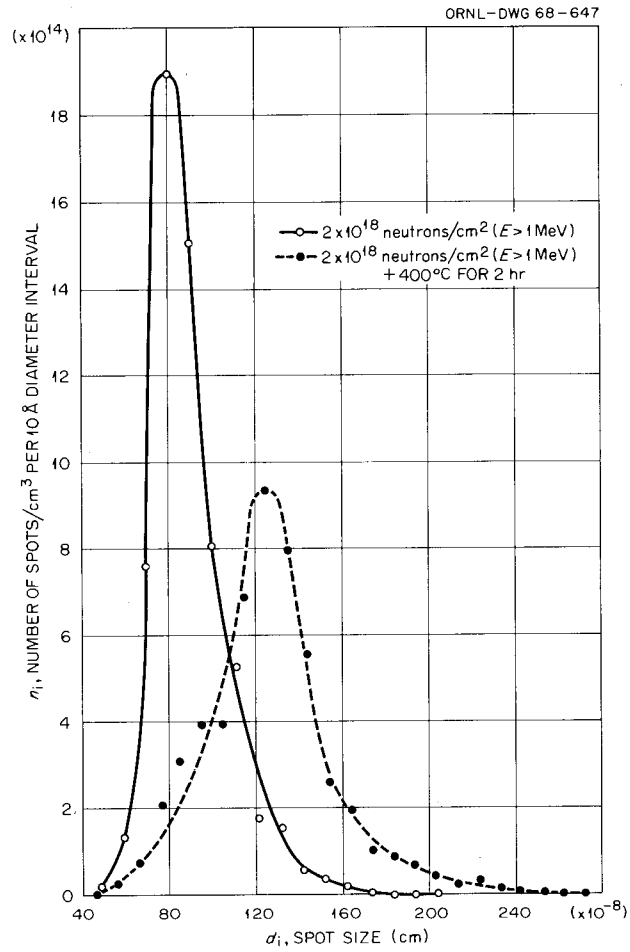
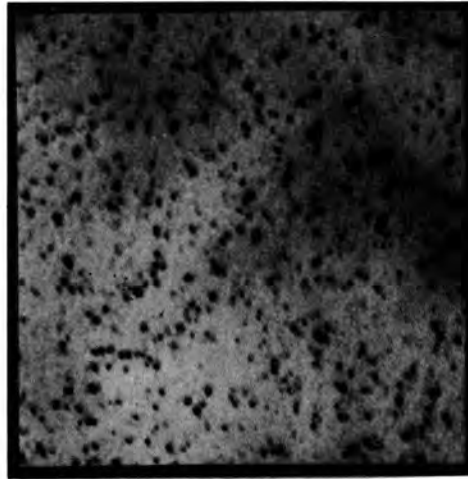
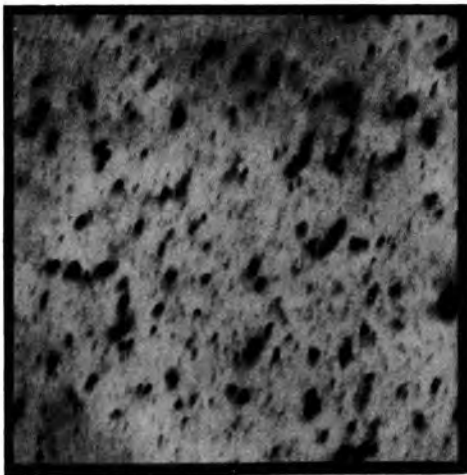


Fig. 25. Defect Size Distribution for Niobium As-Irradiated and After the Post-Irradiation Anneals at Temperatures Indicated.

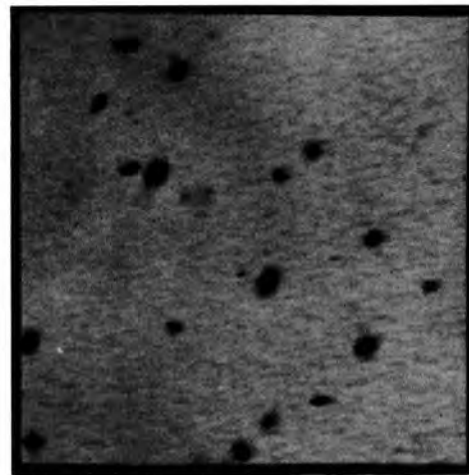
PHOTO 90503



500°C

0.3 μ

600°C



800°C

Fig. 26. Spot Damage in Neutron-Irradiated Niobium After Two-Hour Post-Irradiation Anneals at Temperature Indicated. Fluence, 2×10^{18} neutrons/cm², $E > 1$ Mev.



Fig. 27. Spot Damage in Neutron-Irradiated Niobium After Two-Hour Post-Irradiation Anneal at 600°C Showing Two Types of Defects. The Large Defects have been Denuded in the Vicinity of a Grain Boundary, whereas the Small Defects Show No Denudation.

Following the anneal at 800°C for two hours, most of the defects have annealed out leaving a small number of large defects resolvable in the electron microscope as dislocation loops. We have analyzed these large dislocation loops on the basis of the electron diffraction contrast theory⁵⁸ to determine the nature of the loops. In our analysis, use is

⁵⁸A. Howie and M. J. Whelan, "Diffraction Contrast of Electron Microscope Images of Crystal Lattice Defects," Proc. Roy. Soc., A267, 206, (1962).

made of the stereo techniques in deciding the sense of inclination of loop planes. It is found that the loops of both interstitial and vacancy types are present, the former being somewhat more predominant. We have previously shown evidence that the defects visible in as-irradiated samples are mostly dislocation loops of the interstitial type.⁵⁹ Thus, it is quite reasonable to trace the origin of the large vacancy loops back to the small defects observed after the 600°C anneal.

Discussion

The present work has shown that in niobium containing 38 ppm oxygen and 60 ppm carbon radiation-anneal hardening does not occur in the temperature range at which oxygen atoms are believed to migrate. Instead the hardening is observed in the temperature interval 200-400°C in which carbon atoms are mobile.

Transmission electron microscopy of irradiated and annealed niobium has revealed changes in defect size distribution. We have previously obtained in as-irradiated niobium a reasonable correlation between the defect size distribution on the observed increase in the yield stress, on the basis of the elastic interaction between moving dislocations and the defects.⁵⁹ The predicted increase in the yield stress is

$$\Delta \tau = \frac{G b}{4} (\sum n_i d_i)^{1/2}$$

where G is the shear modulus, b is the Burgers vector, and n_i is the density of defects of size d_i . Based on the defect size distribution

⁵⁹S. M. Ohr, R. P. Tucker, and M. S. Wechsler, "Radiation Hardening in B.C.C. Metals Niobium and Iron," in Proceedings of the International Conference on Strength of Metals and Alloys, Japan Inst. of Metals, (1968).

shown in Fig. 25 for the two hour anneal at 400°C, the increase in the yield stress on annealing is predicted as 0.34 kg/mm² compared to the observed anneal hardening of 8.5 kg/mm². Thus, the changes in the defect size distribution could not account for the anneal hardening.

Two other sources of hardening may be considered, one involves irradiation induced defects too small to be visible in the electron microscope and the other, interstitial impurities. If one accepts that all of the visible defects in the as-irradiated sample are interstitial in nature, vacancies could agglomerate into submicroscopic clusters during post-irradiation anneals. At 400°C these clusters could reach a critical size that is effective in impeding dislocation motion, thus causing the increase in the yield stress. At 600°C these vacancy clusters have grown sufficiently in size so as to become visible for the first time in the electron microscope. Evidence against such a mechanism is found in the work of Williams et al.⁶⁰ The resistivity of one of their samples, containing 30 ppm carbon and less than 3 ppm oxygen, has increased on irradiation, but it decreased well below the pre-irradiation value in the temperature interval 200 to 320°C. This implies that the species migrating in this temperature range is not directly identifiable with radiation induced defects.

The most reasonable interpretation of the present data can be made in terms of interstitial carbon. As was already pointed out, the anneal

⁶⁰J. M. Williams, J. T. Stanley, and W. E. Brundage, "The Interaction of Radiation Produced Defects and Interstitial Impurity Atoms in Niobium," Quarterly Progress Report: Irradiation Effects on Reactor Structural Materials, Nov. 1966-Jan. 1967, BNWL-CC-1053. Pacific Northwest Laboratory, Richland, Washington, 11.18, February (1967).

hardening is observed precisely in the range of temperatures at which carbon atoms are found to migrate.⁶⁰ Another evidence in support of this mechanism is found in our present observations that the unirradiated samples also show a slight increase in the yield stress in this temperature range. After the recrystallization anneal the most of the carbon atoms are expected to have precipitated from the lattice due to extremely low solid solubility in niobium. Evidence exists that carbon is redissolved into the lattice during neutron irradiation.⁶¹ Upon annealing in the range of 200 to 400°C, carbon atoms are expected to migrate to irradiation induced dislocation loops and are trapped there. Transmission electron microscopy has shown that the moving dislocations in neutron irradiated niobium during plastic deformation sweep up the defects thus creating defect free channels.⁶² It appears that the presence of trapped interstitial atoms at the defects creates further difficulty in the sweep-up process and impedes the motion of dislocations.

Fluence Dependence of Radiation Hardening in Polycrystalline Niobium

M. S. Wechsler, R. P. Tucker, and S. M. Ohr

Introduction:

The form of the relationship between the increase in yield stress and neutron fluence has been the subject of some interest, since it provides a direct test of models of radiation hardening. Furthermore, in

⁶¹ J. T. Stanley and W. E. Brundage, "The Interaction of Radiation Produced Defects and Interstitial Impurity Atoms in Niobium," Quarterly Progress Report: Irradiation Effects on Reactor Structural Materials, May-June 1966, BNWL-CC-784. Pacific Northwest Laboratory, Richland, Washington, 10.30, August, (1966).

⁶² R. P. Tucker and S. M. Ohr, "Direct Observation of Neutron Irradiation Damage in Niobium," Phil. Mag., 16, 643, (1967).

connection with the use of structural metals in radiation environments, it is often useful to have a basis for extrapolating the results for low or moderate neutron exposures to the higher exposures anticipated in service. This is especially true today in view of the high exposures appropriate to fast breeder reactor systems. However, the earlier work on the fluence dependence of radiation hardening has been largely devoted to the face-centered cubic metals, especially copper, as was reviewed recently by Makin.⁶³ In this report, we describe some results for the body-centered cubic metal niobium.

The models for radiation hardening are based on the idea that the radiation introduces clusters of defects which act as barriers to dislocation motion. In the dispersed barrier model, the defect clusters are assumed to be scattered at random in the metal lattice with a density proportional to the neutron fluence, at least at low radiation levels. The range of cluster sizes that produces maximum hardening is not known exactly. However, it has been shown^{59,64} that the temperature dependence of the yield stress in niobium is not greatly changed upon neutron irradiation. From this we infer that the clusters are fairly large and thermal vibrations are not effective in assisting dislocations in surmounting them. The clusters responsible for the hardening may therefore be visible by transmission electron microscopy. The

⁶³M. J. Makin, "Radiation Damage in Face-Centered Cubic Metals and Alloys," in Radiation Effects, edited by W. Sheely, Gordon and Breach Science Publishers, Inc., New York, (1968).

⁶⁴S. M. Ohr, R. P. Tucker, and M. S. Wechsler, "Radiation Hardening in B.C.C. Metals Niobium and Iron," Radiation Metallurgy Section Solid State Division Progress Report for Period Ending July 1967, ORNL-4195, 34, (1967).

size distribution of clusters has been determined^{59,64} from electron microscope photographs for two particular fluence levels, 5×10^{17} and 2×10^{18} neutrons/cm² ($E > 1$ Mev). Based on these and a strong-barrier model of radiation, the predicted increases in yield stress upon irradiation were shown to be consistent with those actually observed. In the present study, we report on the measurement of radiation hardening in niobium over a range of fluences from 7×10^{16} to 4×10^{18} neutrons/cm² ($E > 1$ Mev). The shape of the hardening curve is analysed on the basis of several models.

If a cross section σ_B is assigned to the production of the clusters responsible for the radiation hardening, the number produced per unit volume by a fluence Φ may be written as

$$N_V = N \sigma_B \Phi$$

where N is the atomic density. The average spacing of clusters (barriers to dislocation motion) on the slip plane is then

$$l = \frac{1}{(N_V d)^{1/2}} = \frac{1}{(N \sigma_B d \Phi)^{1/2}} \quad (2)$$

to within a geometrical factor⁶⁵ where d is the effective size of the cluster or barrier. In the constant line tension approximation, the breakaway stress σ is given by⁶⁶

$$F = \frac{\sigma}{2} b l \quad (3)$$

⁶⁵J. F. Kocks, "On the Spacing of Dispersed Obstacles," Acta Met., 14, 1629, (1966).

⁶⁶D. K. Holmes, "Radiation Damage in Non-Fissionable Metals," in The Interaction of Radiation With Solids, North Holland Publishing Co., Amsterdam, 1964, 147.

where F is the strength of the barrier. Associating this stress with the increase in stress upon irradiation, $\Delta \sigma$, we have from Eqs. (2) and (3):

$$\Delta \sigma = \frac{2 F}{b} (N \sigma_B d \Phi)^{1/2} \quad (4)$$

which predicts an increase in stress proportional to the square root of the fluence. Despite the simplifications inherent in the derivation of this relation, it is instructive to see how well it is obeyed for the neutron-irradiated niobium under investigation.

Experimental Details:

The starting niobium stock was obtained from CIBA Corporation in the form of niobium powder. The powder was drop cast, given several electron-beam zone passes, and rolled to 5-mil sheet from which tensile samples, 4.2 mm wide and 12.7 mm gage length, were stamped out. The samples were then given a recrystallization anneal at 1050°C, which produced a grain size of about 44 μ . The photomicrograph in Fig. 28 shows the grain structure. A chemical analysis of the recrystallized material is given in Table 5.

The samples were irradiated for various lengths of time in Tube 12 of the Hydraulic Facility of Position F-8 in the Oak Ridge Research Reactor. The neutron flux as determined by nickel monitors was 2.0×10^{13} neutrons per cm^2 sec ($E > 1$ Mev) and the irradiation temperature was below 50°C. Following a waiting period for radioactive decay, the samples were tested at room temperature at a crosshead speed of 0.01 cm/min which corresponds to a strain rate of 1.3×10^{-4} sec $^{-1}$.

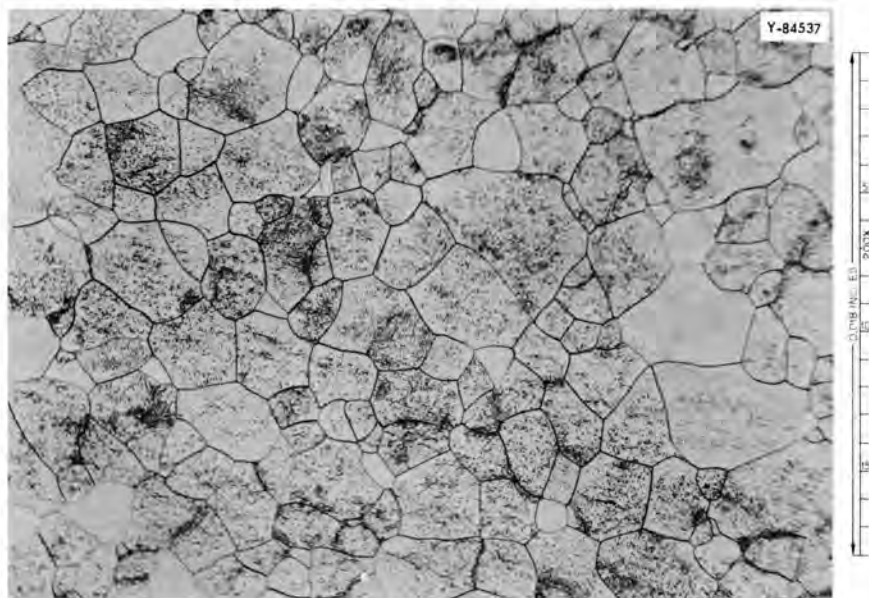


Fig. 28. Grain Structure in Niobium After Recrystallization at 1050°C for 1 Hour. Etch Pits are Observable in Most Grains. Etchant: 10 Parts HF, 10 Parts H₂SO₄, 10 Parts H₂O, 1 Part H₂O₂.

Results:

Figure 29 shows the stress-strain curves as a function of neutron fluence. The irradiation causes an increase in upper and lower yield stresses and a decrease in uniform and fracture strains. These effects are significant even at fluences below 10^{17} neutrons/cm² ($E > 1$ Mev).

The dependence of the increase in the upper and lower yield stresses on neutron fluence is illustrated in Fig. 30. Each point represents the average value of several determinations for each fluence level. It is seen that the increase in yield stress is proportional to the square root of the fluence, as predicted by Eq. (3), only for the measurements at the lower fluences (below about 10^{18} neutrons/cm² $E > 1$ Mev). At higher fluences, the yield stress increases less rapidly.

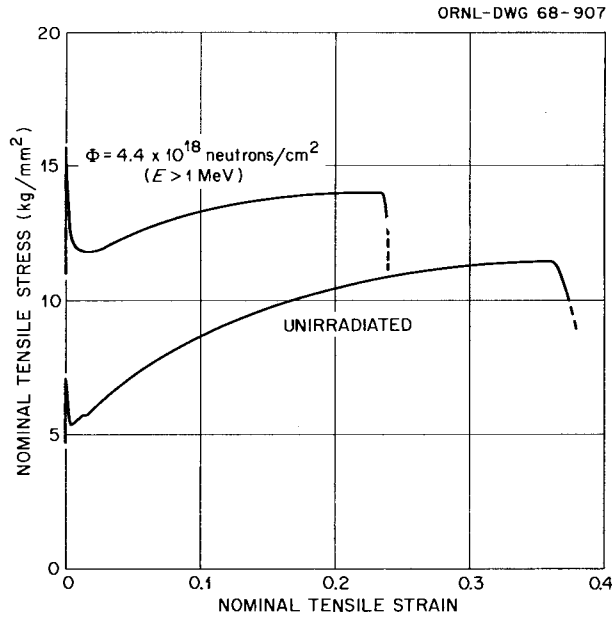


Fig. 29. Stress-Strain Curves for Polycrystalline Niobium Sheet Samples Tested in Tension at 25°C.

Table 6

RADIATION HARDENING IN NIOBIUM

b, Burgers vector, {110} <111> slip	2.85 Å
Nb^3 , N = atomic density	1.30
G, shear modulus, {110} <111>(Ref. 58)	4280 kg/mm ²
B, Eq. (5) and Fig. 30	$0.58 \times 10^{-8} \left(\frac{\text{kg}}{\text{mm}^2}\right) \cdot \text{cm}$
σ_B , barrier production cross section, using d = 80 Å (text)	
(1) infinitely strong barriers, $F = 0.8 \text{ Gb}^2$ (Refs. 59,64)	0.02 barns
(2) loop hardening, $F = 0.25 \text{ Gb}^2$ (Refs. 59,64)	0.2 barns
σ_C , cluster production cross section (Ref. 62)	0.04 barns
σ_S , neutron scattering cross section (Ref. 71)	8 barns

Discussion:

The curves drawn through the experimental points in Fig. 30 indicate two straight line portions. It is reasonable to assume that the initial portions of the curves correspond to hardening of the type described by Eq. (4). In this case, the slope, B, of the initial line is given by

$$B = \frac{2F}{b} (N \sigma_B d)^{1/2} \quad (5)$$

From Fig. 30 we find $B = 0.58 \times 10^{-8}$ (kg/mm²). cm for the lower yield stress. As we have said, the cluster size critical to radiation hardening is not well known. However, if we choose a size near the size observed by transmission electron microscopy, the cross section σ_B may be calculated from (5) and compared to other pertinent cross sections (Table 6). The observations of Tucker and Ohr⁶⁷ indicated that the cluster size distribution peaks at about 80 Å for $\Phi = (0.5 - 2.0) \times 10^{18}$ neutrons/cm² (E > 1 Mev); hence we take $d = 80$ Å. Now, for infinitely strong barriers, Kocks⁶⁸ and Foreman and Makin⁶⁹ have shown that $F = 0.8 Gb^2$, where G is the shear modulus. On the other hand, Ohr et al.^{59,64} have indicated that for loop hardening $F = 0.25 Gb^2$. A calculation of G for {110}<111> shear based on the room temperature

⁶⁷R. P. Tucker and S. M. Ohr, "Direct Observation of Neutron Irradiation Damage in Niobium," Phil. Mag., 16, 643, (1967).

⁶⁸U. F. Kocks, "A Statistical Theory of Flow Stress and Work Hardening," Phil. Mag., 13, 541, (1966).

⁶⁹A. J. E. Foreman and M. J. Makin, "Dislocation Movement Through Random Arrays of Obstacles," Phil. Mag., 14, 911, (1966).

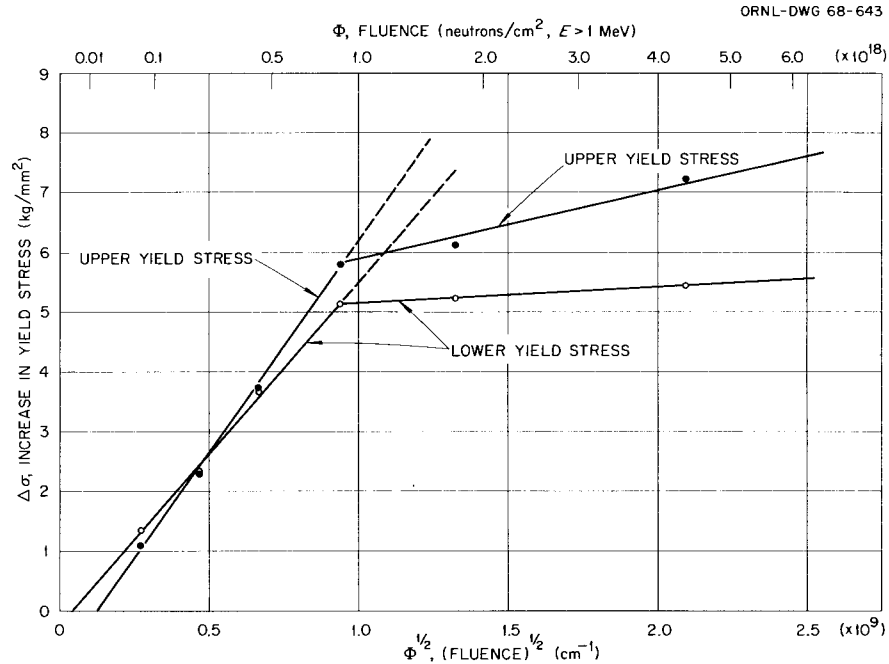


Fig. 30. Increase in Yield Stress Versus $\Phi^{1/2}$ for Polycrystalline Niobium, Showing Straight Line Fit to Low- Φ Portion. Irradiation Temperature, $<50^\circ\text{C}$. Test Temperature, 25°C .

elastic constants given by Carroll⁷⁰ gives $G = 4280 \text{ kg/mm}^2$. As indicated in Table 6, the σ_B deduced from these considerations are 0.02 and 0.2 barns for infinitely strong barriers and for loop hardening, respectively. It is difficult to tell at this time how reasonable these σ_B values are. However, it is interesting that these cross sections bracket the cross section for the production of clusters visible by transmission electron microscopy, i.e. the value $\sigma_c = 0.04$ barns deduced from Tucker and Ohr's observation⁶⁷ that 5×10^{15} clusters/cm³ are present in a foil irradiated to 2×10^{18} neutrons/cm²,

⁷⁰K. J. Carroll, "Elastic Constants of Niobium from 4.2° to 300°K," J. Appl. Phys., 36, 3689, (1965).

$E > 1$ Mev. It is of interest, also, to compare these cross sections with the neutron scattering cross section⁷¹ of about 8 barns. Since the σ_B 's fall between 0.02 and 0.2 barns, we conclude that only one barrier is produced per 40 - 400 neutron collisions.

A further point illustrated in Fig. 30 is the reduced slope for $\dot{\phi} \approx 10^{18}$ neutrons/cm². A saturation in the rate of hardening has been observed previously for FCC metals^{72,73} and is one of the puzzling features of radiation hardening since it occurs at $\dot{\phi}$ levels too low to be explained easily in terms of overlap of clusters. Another possibility has been treated by Varley.⁷⁴ In a kinetic analysis of the nucleation and growth of clusters, he showed that a time is reached at which no new loops are formed while those already present grow in size.

Still another possibility is that the strength of the barriers depends upon the formation of complexes between defect clusters and interstitial impurities. Williams et al.⁷⁵ have shown that the annealing stage at about 150°C in irradiated niobium is associated with the motion

⁷¹D. J. Hughes and R. V. Schwartz, "Neutron Cross Sections," BNL-325, 201-202, (1958).

⁷²M. J. Makin, "Radiation Damage in Face-Centered Cubic Metals and Alloys," in Radiation Effects, edited by W. Sheely, Gordon and Breach Science Publishers, Inc., New York, (1968).

⁷³M. J. Makin and F. J. Minter, "Irradiation Hardening in Copper and Nickel," Acta Met., 8, 691, (1960).

⁷⁴J. H. O. Varley, "The Agglomeration into Clusters of Interstitial Atoms and Vacancies Generated by Fast Neutron Irradiation," Phil. Mag., 7, 301, (1962).

⁷⁵J. M. Williams, W. E. Brundage, and J. T. Stanley, "The Effect of Oxygen on 'Stage III' Annealing in Neutron-Irradiated Niobium," to be published in Metals Science Journal.

of interstitial oxygen to radiation-produced clusters. Also, the radiation anneal hardening discussed in another section of this report⁷⁶ indicates that the motion of interstitial impurities to defect clusters is responsible for an additional increment of hardening upon annealing. It might be suggested that defect-impurity aggregation takes place early in the irradiation in the present experiments. This process requires a species of interstitial impurity mobile at the irradiation temperature (below 50°C) and on the exhaustion of the supply of these at fluence levels of about 10^{18} neutrons/cm². Perhaps hydrogen is a possibility, since it is known to be introduced easily into refractory metals⁷⁷, and is likely to be mobile at the temperature of irradiation.

Deformation of Irradiated and Unirradiated Nb Single Crystals in Compression

H. D. Guberman and R. E. Reed

The present investigation was undertaken to evaluate the effect of neutron irradiation upon the deformation characteristics of niobium. In particular, we wished to determine how the increase in flow stress upon neutron irradiation was apportioned between the thermal and athermal components of stress. Such information is necessary for developing detailed models which will enable us to understand the nature of radiation-induced hardening. In this report we present the results of testing at 194°K, 298°K and 525°K for unirradiated Nb and samples irradiated to 1.1×10^{17} and 8.3×10^{17} n/cm², $E > 1$ Mev.

⁷⁶G. M. Ohr, R. P. Tucker, and E. D. Bolling, "The Annealing Characteristics of Neutron Irradiated Niobium," this report.

⁷⁷G. D. Westlake and W. R. Gray, "A Pitfall in the Preparation of Metal-Hydrogen Alloys for Transmission Electron Microscopy," Appl. Phys. Lett., 9, 3-4, July (1966).

The material used in this investigation was notably purer than that used in prior studies of the properties of Nb.⁷⁸ Single crystals were grown by an electron-beam floating zone technique which involved three passes of the molten zone. The starting material was a CIBA stock which was particularly low in Ta and W.⁷⁸ The resistivity ratio of the material between room temperature and 4.2°K ranged between 471 and 494. The crystals were grown with a $\langle 491 \rangle$ rod axis such that the maximum resolved shear stress fell on the $\{110\}\langle 111 \rangle$ slip system.

Compression samples were cut from the zoned rod by a spark erosion process utilizing a 0.25 mm Cu wire as the cutting tool and the No. 6 spark setting of the Servomet spark machine. The ends of the samples were lapped by hand until they were flat and parallel to within 0.06°. The samples were then lightly polished in a solution of HF:HNO₃ (1:4) chilled in an ice and water bath to reduce the possibility of charging with hydrogen. The sample dimensions after fabrication were typically 9.5 mm in length and 4.3 mm in diameter.

Irradiations were performed in the Hydraulic Facility of the Oak Ridge Research Reactor with the samples shielded by cadmium tubing about 1.2 mm in thickness. The irradiation temperature was $88^\circ \pm 5^\circ\text{C}$. The samples were stored at room temperature for about two weeks to allow the radioactivity to decay prior to testing.

⁷⁸R. E. Reed, this report.

All the compression tests were carried out on a floor model Instron testing machine in a fixture designed to ensure axially of loading. The crosshead speeds were varied between 0.02 in/min and 0.002 in/min for strain-rate change measurements. The stress measurements reported here are from the higher strain rate. The samples were tested in air at room temperature and in an oil bath (Dow-Corning Silicone Oil No. 200, viscosity 50 cs) which was also used as the high temperature bath. At elevated temperatures the oil was heated by thermistor controlled electric immersion heaters to the desired temperature. The lower temperature was achieved by a dry-ice and acetone bath. During testing the fluids were constantly stirred to ensure uniformity of temperature distribution. During the high temperature tests, the oil bath and the compression jig were first raised to the testing temperature and then the sample was inserted in order to minimize the time at an elevated temperature. The samples normally reached the yield point within four minutes after immersion and the entire test was completed after about seven minutes.

The results of the mechanical testing are summarized in Table 7 and the pertinent data are displayed in Fig. 31. The data show a significant temperature dependence of the yield stress which is somewhat affected by the neutron irradiation. The high temperature tests were carried out at a temperature which, according to Conrad,⁷⁹ is in the

⁷⁹H. Conrad, "The Relation Between the Structure and Mechanical Properties of Metals," Proceedings of the Conference held at the National Physical Laboratory, Teddington, Middlesex, 503, January (1963).

Table 7

SUMMARY OF MECHANICAL MEASUREMENTS+

	Temp.	Flow Stress	
		L.Y.S. (kg/mm ²)	U.Y.S. (kg/mm ²)
Non-Irrad.	298°K	1.63 ± .06	-
1.1 x 10 ¹⁷ n/cm ²	298°K	2.25 ± .07	2.89 ± .03
8.3 x 10 ¹⁷ n/cm ²	298°K	2.98 ± .04	3.8 ± .4
Non-Irrad.	500° - 525°K	0.286 ± .005	-
1.1 x 10 ¹⁷ n/cm ²	525°K	1.00 ± .04	1.05 ± .02
8.3 x 10 ¹⁷ n/cm ²	525°K	1.26 ± .04	1.64 ± .02
Non-Irrad.	194°K	9.28 ± .04	-
1.1 x 10 ¹⁷ n/cm ²	194°K	12.2 ± .2	12.7 ± .4
8.3 x 10 ¹⁷ n/cm ²	194°K	12.5	16.1

+All stresses are resolved shear stresses

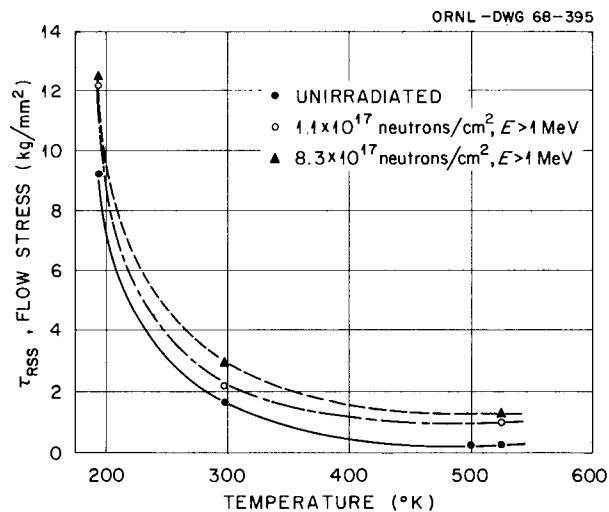


Fig. 31. Yield Stress vs Temperature as a Function of Neutron Irradiation for Compression Tests on High-Purity Nb Single Crystals.

region where the thermal component of stress (also known as the effective stress) has been reduced to zero leaving only the athermal component, i.e. that which is associated with long range dislocation interactions. The high temperature data indicates that neutron irradiation has a significant effect upon the athermal component of stress. However, the non-parallel relationship of the curves in Fig. 31 suggests that there is also an effect upon the thermal component of stress especially at lower temperature.

Measurements were also made of the activation volume V^* , a parameter of interest from the thermal activation theory of deformation. The activation volume may be defined by the following expression.

$$\frac{V^*}{kT} = \frac{\ln \dot{\epsilon}}{\tau^*} T$$

where $\dot{\epsilon}$ is the strain rate, τ^* is the effective stress and the other symbols have their usual meanings. This parameter may also be related to the microscopic size and spacing of the obstacles to dislocation motion. The activation volume was determined with respect to strain as a function of temperature and radiation fluence (Figs. 32 and 33).

At room temperature v^* appears to be independent of strain and slightly higher than the value found earlier for niobium grown in different ways from other starting material.⁸⁰ At 194°K v^* appears to have a tendency to decrease with strain. It is interesting to note that at 525°K where presumably the effective stress has been reduced

⁸⁰R. W. Armstrong, R. E. Reed, and H. D. Guberman, "Characterization of the Strain Rate Dependence of the Shear Stress for Niobium Single Crystals," Scripta Met., 1, 1257, (1967).

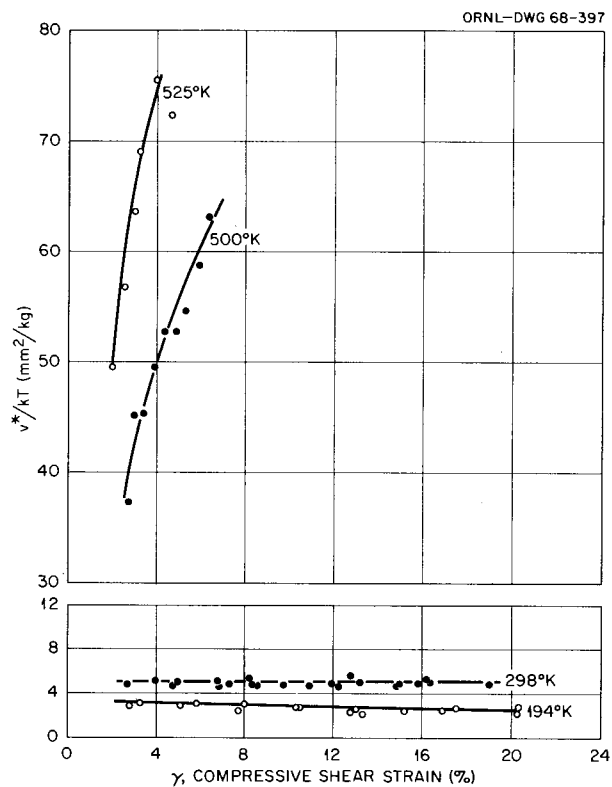


Fig. 32. Activation Volume vs Shear Strain as a Function of Temperature for Unirradiated High Purity Nb Single Crystals.

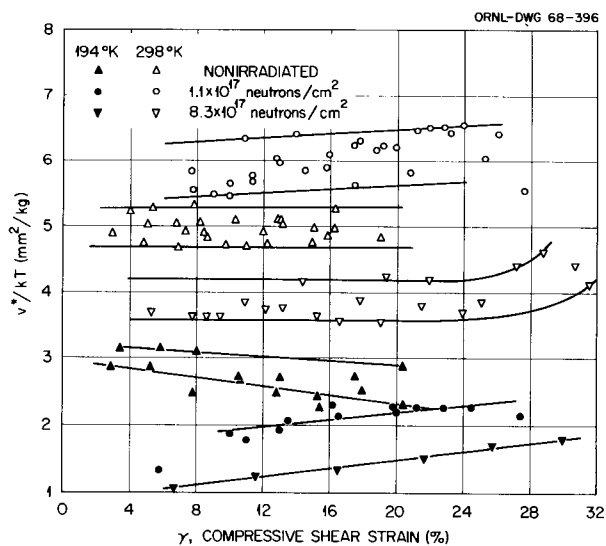


Fig. 33. Activation Volume vs Shear Strain as a Function of Temperature and Neutron Dose for High Purity Single Crystal Nb.

to zero and consequently there ought to be no effect of a change in strain rate, all the samples still showed a measurable strain-rate sensitivity. The effect has been reduced an order of magnitude as evidenced by the extremely high values of v^* . Of further interest is the significant increase in v^* with increasing strain.

The observation of strain-rate sensitivity at a temperature where one would expect it to be absent might be taken as evidence that the effective stress had not been reduced to zero and that consequently, we are not observing the athermal component of stress, τ_G . However, the measurements on the unirradiated Nb indicate that the yield stress is no longer changing with temperature in this temperature range. Therefore, it seems reasonable to accept this value of the stress as the athermal component of stress. The observed strain rate dependence might then be accounted for by the argument that the mobile dislocation density is not remaining constant during the strain rate change as is commonly assumed.⁸¹ At lower temperatures this phenomenon would be unobserved because the relatively large effective stress is already acting to produce a strain rate sensitivity.

Neutron irradiation significantly affects the activation volume at 298°K and 194°K (Fig. 33). At room temperature the lower radiation dose increases v^* while the higher dose decreases v^* . At 194°K the value of v^* is decreased progressively as the dose is increased. These references

⁸¹J. W. Christian, "A Comment on the Relation Between Dislocation Velocity and Effective Flow Stress," Acta Met., 15, 1257, (1967).

pertain particularly to the value of v^* at the lower yield point or initial flow stress. It is noteworthy that the slopes of the $v^* - \gamma$ curves are significantly changed especially at the low temperature, after irradiation.

These changes in the activation volume are entirely consistent with the values of the effective stress, τ^* , determined from the flow stress measurements (Table 8). It has been well established that the activation volume decreases as the effective stress increases.⁸² Thus the increase and decrease in v^* at room temperature for the lower and higher doses is accompanied by a decrease and increase in τ^* . Similarly at 194°K, the decreasing v^* is accompanied by an increase in τ^* as the neutron dose is increased. This shows quite clearly that there is an effect of neutron irradiation upon the effective stress. At 298°K it is not as large as the effect on the athermal component of stress, but it is larger than the change in the athermal component at 194°K (Table 8).

At the present time no effort will be made to interpret these results except perhaps to point out that there may be some correlation with observations of defects in neutron irradiated Nb by transmission electron microscopy.⁸³ Small dislocation loops were found after doses greater than about 5×10^{17} n/cm² ($E > 1$ Mev) but not at doses lower

⁸²H. Conrad, "The Relation Between the Structure and Mechanical Properties of Metals," Proceedings of the Conference held at the National Physical Laboratory, Teddington, Middlesex, 503, January (1963).

⁸³R. P. Tucker and S. M. Ohr, "Direct Observation of Neutron Irradiation Damage in Niobium," Phil. Mag., 16, 643, (1967).

than that. Note that this falls between the two doses used in this experiment. An obvious extension of this work is to subject the samples tested to examination by transmission electron microscopy.

Table 8
Athermal and Thermal Components of Stress+

	τ_G (kg/mm ²)	$\tau^*_{298^\circ\text{K}}$ (kg/mm ²)	$\tau^*_{194^\circ\text{K}}$ (kg/mm ²)
Non-Irrad.	0.29	1.34	9.0
1.1×10^{17} n/cm ² , E > 1 Mev	1.00	1.25	11.2
8.3×10^{17} n/cm ² , E > 1 Mev	1.26	1.72	12.2

+All stresses are resolved shear stresses

Spark-Machining Damage in Niobium Single Crystals
as Indicated by Etch Figures

H. D. Guberman

The preparation of metallic single crystals for research purposes by electric spark-machining has become increasingly popular. Numerous references, however, have already been made to various aspects of physical damage introduced by this technique, for example, the depth of damage in 70:30 brass⁸⁴ the formation of cleavage cracks in tungsten and molybdenum^{85,86}, the temperature rise in the vicinity of a spark-cut,⁸⁷ and residual stresses in a spark-cut surface.⁸⁸ The latter reference also discusses phase changes and reviews the nature of spark-machined surfaces in general. In this note we report some observations concerning the distribution of dislocations in the vicinity of a spark-machined notch in single crystals of niobium.

⁸⁴L. E. Samuels, "Surface Damage Produced by the Electric-Spark Cutting Process," J. Inst. Metals, 91, 191, (1962).

⁸⁵P. Beardmore and D. Hull, "Nucleation of Cleavage Cracks in Tungsten and Molybdenum by Spark-Machining," J. Inst. Metals, 94, 14, (1966).

⁸⁶L. Van Someren, "Cleavage Cracks Induced by Spark Machining," J. Inst. Metals, 94, 368, (1966).

⁸⁷J. R. Hancock, J. G. Grosskreutz, and C. Q. Bowles, "Note on Specimen-Temperature Rise During Electric-Spark Cutting of Aluminum and Copper," J. Inst. Metals, 94, 74, (1966).

⁸⁸H. K. Lloyd and R. H. Warren, "Metallurgy of Spark-Machined Surfaces," J. Iron Steel Inst., 203, 238, (1965).

Samples were sectioned by a spark-cutting device (see below) from a 1/2-inch-diameter single crystal with its longitudinal axis parallel to the $\langle 111 \rangle$ direction such that the surfaces to be studied were normal to the $\langle 111 \rangle$. The crystals were grown from a seed by an electron-beam floating zone process.⁸⁹ After sectioning, the samples were deeply polished in HF:HNO₃ (1:4) until a highly polished disc approximately 3-4 mm in thickness remained. A notch was then cut into the sample normal to the $\langle 111 \rangle$ axis using the Servomet spark-machine on No. 4 and No. 6 spark settings. Kerosene was used for the dielectric fluid. A locally designed device using 0.25 mm copper wire moving at a speed of about 5.3 cm/min was the cutting tool. The sample was then chemically etched after a carbon decoration treatment⁹⁰ to enable the grown-in dislocation substructure and spark-induced dislocation configurations to be observed by optical microscopy. For comparison, a notch was also introduced mechanically into a sample with a Gillings-HamCo thin sectioning machine and a 0.2 mm SiC wheel rotating at 6500 rpm.

In each case the distribution of dislocations in the vicinity of the cut was generally like that indicated in Fig. 34. The major features are zones of plastic deformation that extend beyond the notch in the direction of cutting. The directions about which these plastic zones appear to be symmetrically arranged lie approximately 40° to 50° from the direction of cutting. A region of extremely high dislocation density, such that etch figures cannot be resolved, is found adjacent to

⁸⁹R. E. Reed, "Electron Beam Floating Zone Refining of Niobium," in Proceedings of the Second International Conference on Electron and Ion Beam Science and Technology, April 17-20, 1966, Gordon and Breach Publishers, New York. To be Published.

⁹⁰H. D. Guberman, "Stress Dependence of Dislocation Velocity in Single Crystal Niobium," Acta Met., in press.

the cut surface at the root of the notch (Figs. 35 and 36). In the case of the No. 4 spark only, this region of extremely high dislocation density was found along the entire boundary of the cut. Numerous slip traces extending far beyond the area of view in Fig. 35 were observed in the case of the No. 4 spark. The depths of damage observed in the above examples are summarized in Table 9. The dimensions were determined either from the furthest extent of recognizable slip traces or from the depth at which the dislocation density became equal to the average initial density in the matrix.

From these observations it is apparent that the damage decreases as one decreases the spark energy. Therefore, it is very likely that one may be able to reduce the damage even further, if it is necessary in a given situation, by operating at a still lower spark energy. It is also interesting to note that the damage produced by a careful mechanical cutting operation does not compare unfavorably with that produced by spark-machining in the intermediate spark range.

The high density of dislocations in the vicinity of the spark-cut surface gives evidence of the severity of the treatment the surface receives. Undoubtedly, some of the deformation is associated with the thermal stresses produced by the quenched material at the spark-produced crater.⁸⁸ However, the depth of penetration of the deformation and the particular distribution of the dislocations indicate that shock waves of considerable amplitude (especially at the higher spark energies) are generated and propagate through the bulk material.

Table 9

SUMMARY OF DEPTH OF DAMAGE ASSOCIATED WITH CUTTING^a

	<u>a (mm)</u>	<u>b (mm)</u>
No. 4 Spark	0.75	1.5
No. 6 Spark	0.04	0.22
Cut-Off Wheel	0.15	0.40

^aThese dimensions were measured in the regions shown in Fig. 34.

ORNL-DWG 67-12797

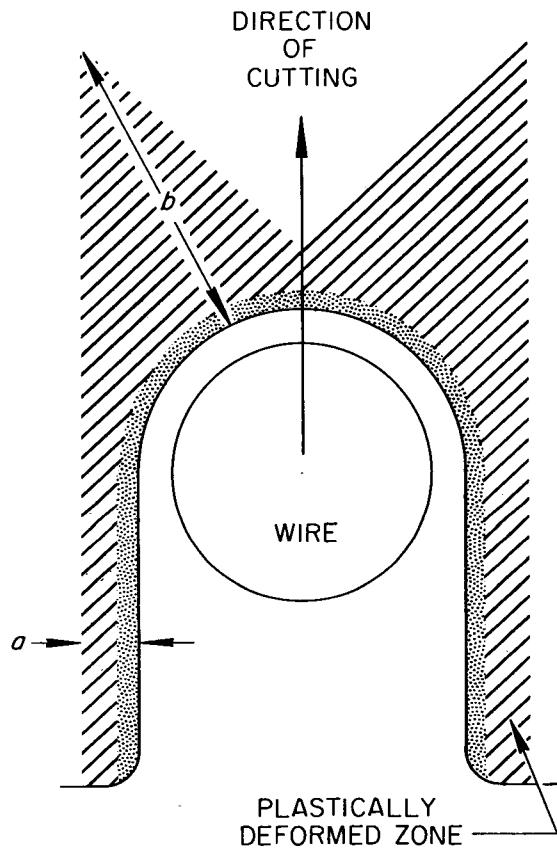


Fig. 34. Schematic of Spark-Cut Notch and the Region of Plastic Deformation.

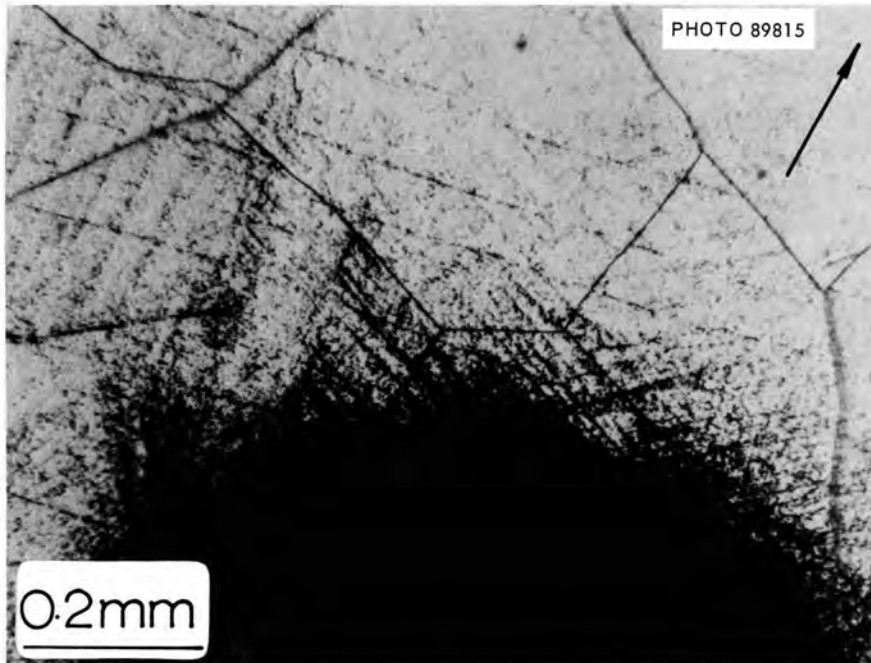


Fig. 35. Etch Pattern of the Root of the Notch Produced by No. 4 Spark on the Servomet Spark Machine. The Arrow Indicates the Direction of Motion of the Cutting Tool. Sub-Grain Boundaries and Spark-Induced Slip Traces are Observable.

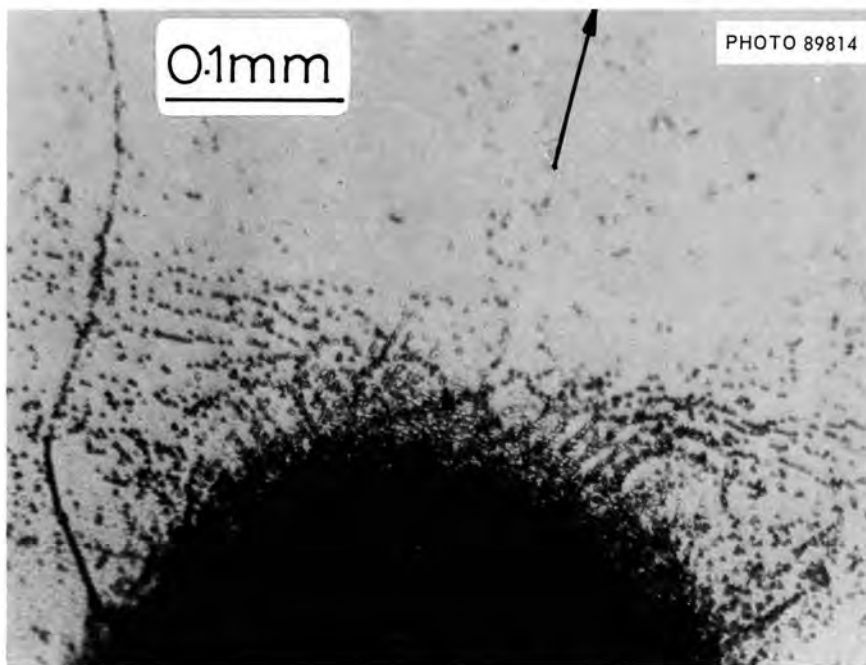


Fig. 36. Etch Pattern at the Root of the Notch Produced by a No. 6 Spark.

Evaluation of Niobium Source Materials Suitable for
Electron Beam Float Zone Melting*

R. E. Reed, R. P. Tucker, and C. L. Brooks

Niobium metal from three sources was electron beam float-zone melted (EBFZM) in an evaluation test to find a suitable starting material for purification and growth of single crystals. Prior work⁹¹ had shown that it was important to obtain a starting material low in Ta and W since these two metallic impurities could not be removed from niobium by the EBFZM technique. An initial evaluation⁹² of niobium starting material prepared by electrodeposition from a molten salt⁹³ revealed that this type material was very promising as a source of low Ta and W niobium metal. However, it generally was received as a powder or porous chips and required an additional consolidation step to obtain a rod form suitable for EBFZM. This report describes the material characterization results obtained on Wah Chang Corp. electron beam drip melt ingot, DuPont Co. D3 granules, and CIBA Ltd dendritic powder after purification and crystal growth using a practical standard EBFZM schedule.

*Work performed under the Research Materials Program.

⁹¹R. E. Reed, "The Preparation and Purification of Single Crystals of Niobium," Radiation Metallurgy Section Solid State Division Progress Report for Period Ending February 1966, ORNL-3949, 35, (1966).

⁹²R. E. Reed, "Niobium: Purification and Perfection," Radiation Metallurgy Section Solid State Division Progress Report for Period Ending January 1967, ORNL-4097, 20, (1967).

⁹³G. W. Mellors and S. Senderoff, "Electrodeposition of Coherent Deposits of Refractory Metals: I. Niobium," J. Electrochem. Soc., 112, 266, (1965).

Experimental Procedure

A. Starting Materials:

The starting materials will be described separately as each had a different handling schedule for obtaining a rod form suitable for EBFZM.

1. Wah Chang Corp. Electron Beam Melted Ingot. --A 1-inch diameter bar, 3-ft long, which was formed from a 3-in. diameter electron beam drip melted ingot was purchased from Wah Chang Corp., Albany, Oregon. This rod was cold swaged down to 4.8-mm diameter. Rods were prepared for EBFZM by cutting to length, chemical polishing, washing in distilled water, and air drying. The chemical analyses for this material are listed in Table 10.

2. DuPont Co. D3 Granules. --Fifty pounds of niobium D3 granules were purchased from E. I. DuPont de Nemours and Co., Pigments Department, Wilmington, Delaware. The granules were consolidated by drop casting into 5/8-in. diameter rod, 5-in. long, using arc melting. This resulted in an increase in both the Ta and W impurity levels due to the Ta striking peg and W tipped electrode present in the arc casting furnace. The drop cast ingot was then cold swaged to 4.8-mm diameter rod. These rods were then prepared in the same way as the Wah Chang material for EBFZM. The chemical analyses for this material are also listed in Table 10.

3. CIBA Dendritic Powder. --Ten pounds of dendritic niobium powder was purchased from CIBA Ltd., Basle, Switzerland. This material had been prepared by electrodeposition from a molten salt. It was characterized by a low Ta and W content and a high Na content, as determined by neutron activation analysis. In order to avoid Ta and W contamination, the following schedule was used to consolidate this powder.

Table 10

Chemical Analyses of the Niobium
Starting Material Prior to EBFZM

Element	Material Source		
	Wah Chang wt. ppm	DuPont wt. ppm	CIBA wt. ppm
C	42	50	48
O	120	110	20
N	46	10	16
H	5	15	3
Ta	350	321	22
W	274	89	3
Fe	20	20	6
Zr	60	<1	<1
Cr	6	20	6
Ni	<1	80	8
Cu	<1	<1	3

Note: All other elements undetected or less than 1 wt. ppm.

a) The powder was packed into 5/8-in. diameter copper tubing which had been carefully cleaned and etched.

b) The tube was evacuated with a liquid nitrogen trapped mechanical pump and sealed under vacuum.

c) It was then cold swaged down to approximately 5/16-in. diameter.

d) After etching off the copper tubing, a niobium powder rod compact was obtained about 5-mm diameter and strong enough to EBFZM.

e) This powder compact was then zone melted for one pass in 5×10^{-6} torr at a zone speed of about 20 cm/hr. It was found that out-

gassing passes in the solid state were ineffective in preventing "spitting" when the molten zone was formed. Thus, the powder compact was melted completely through on the first pass.

f) A second pass was then made at 5×10^{-7} torr vacuum and 20 cm/hr zone speed.

g) The as-zoned rod was cold swaged to 4.8-mm diameter rod. This was done to obtain a constant diameter rod.

h) The as-swaged rod was prepared for EBFZM in the same manner as the other two starting materials.

The chemical analyses for this material are given in Table 10.

B. EBFZM Procedure:

All of these starting materials were further purified using a practical standard EBFZM procedure. High-purity as-zoned niobium single crystals with a resistance ratio $\left[R_{300^\circ\text{K}}/R_{4.2^\circ\text{K}(15 \text{ kgauss})} \right]$ equal to 1400 have been previously grown.⁹² However, this involved multipasses (10 passes) and high vacuums (8×10^{-10} torr). It was considered desirable to attain high purities using a more practical EBFZM schedule. The following procedure was used.

1. The specimen and a seed crystal were loaded into the electron beam zone refiner (Materials Research Corp. Model EBZ-94) which was equipped with a Viton O-ring on the stainless steel bell jar Wheeler seal. All other seals were copper gaskets.

2. The system was evacuated overnight without a bake, using a liquid nitrogen trapped 10-in. diffusion pump with a water baffled 4-in. diffusion pump as a booster pump. The base pressure attained was 5×10^{-8} torr.

3. Three zone passes were made on the 4.8-mm diameter rod over a 18-cm length, using a zone speed of 10 cm/hr. The vacuum was 3×10^{-7} , 1×10^{-7} , and 5×10^{-8} torr during the first, second, and third pass, respectively.

4. For some of the CIBA material, the first pass was made in a vacuum containing 1×10^{-5} torr oxygen. This was done by using a variable leak connected to a pure oxygen supply. The leak rate was adjusted to maintain 1×10^{-5} torr pressure on the ion gage. The second and third pass was made with the variable leak closed in a vacuum of 1×10^{-7} and 5×10^{-8} torr, respectively.

C. Annealing Procedure:

Some of the as-zoned rods were further treated in a high-vacuum annealing furnace. A bakeable stainless steel chamber was evacuated using a 6-in. diffusion pump trapped with first a water cooled baffle and then a liquid nitrogen cooled trap. The foreline of the pump contained a 2-in. diffusion booster pump which had a water baffle on it. A bakeable r.f. 20 KW power feedthrough was used to place an induction coil in the center of the chamber. The specimens were hung in the center of the coil with a split Ta radiation shield between them and the coil.

A typical annealing sequence would be :

1. Place the samples in the chamber and pump it to about 5×10^{-8} torr vacuum.
2. Bake the stainless steel chamber overnight at 250°C .
3. The pressure after cooling the chamber will be about 5×10^{-9} torr. The specimens are then annealed at 2350°C , as measured by an optical micropyrometer, for 5 hours. The pressure at the start of the

anneal was about 1×10^{-7} torr and near the end of the anneal about 2×10^{-9} torr.

4. The r.f. power was shut off quickly at the end of the anneal.

D. Material Characterization:

The rods were examined for purity using several methods. Direct methods were chemical analyses such as neutron activation analyses for Ta and W, vacuum fusion analyses for O, N, and H, Leco combustion analyses for C, and spark source mass spectrographic analyses for other metallic impurities. Indirect methods were: resistance ratios measured between room temperature and liquid helium temperature in a 15 kilogauss magnetic field; and a flow stress measured at the lower yield point of the resolved stress-strain tensile curve. The tensile specimens were prepared by centerless grinding and chemical polishing as described in a previous report.⁹⁴ The tensile testing was done at room temperature on a table model Instron machine at a strain rate of 1.7×10^{-4} sec⁻¹. The specimens were oriented with the tensile axis near $\langle 491 \rangle$ such that the Schmid factor for slip on the (101) $[\bar{1}11]$ system was 0.5.

Experimental Results

Table 11 summarizes the chemical analyses obtained on the three starting materials after the various purification steps. Comparing these data with those in Table 10, it is evident that the three-pass EBFZM schedule had little effect upon the carbon content of the starting materials. However, the oxygen and nitrogen content of the Wah Chang

⁹⁴R. E. Reed, "Effect of the Number of Zone Passes on the Flow Stress of Niobium Single Crystals," Radiation Metallurgy Section Solid State Division Progress Report for Period Ending July 1966, ORNL-4020, 23, (1966).

Table 11. Chemical Analyses of Niobium after Various Purification Steps

Material Source	Spec. No.	Treatment	Chemical Analysis (wt. ppm)										
			C	O	N	H	Ta	W	Fe	Cr	Ni	Zr	Cu
Wah Chang	58d	Zoned	42	22	4	2	356	268	6	6	<1	20	1
	59d	Zoned & Annealed	32	25	3	1	309	233	<1	<1	<1	6	<1
DuPont	D12d	Zoned	42	14	3	1	313	88	<1	6	3	<1	3
	D13d	Zoned & Annealed	30	35	3	4	272	74	<1	<1	<1	<1	<1
CIBA	C14d	Zoned	51	27	8	2	21	2	<1	<1	<1	<1	<1
	C20d	Zoned (oxygen)	27	27	8	2	17	2	<1	<1	<1	<1	<1
	C21d	Zoned (oxygen) & Annealed	44	32	1	2	20	2	<1	<1	<1	<1	<1

and DuPont material was appreciably reduced. In the case of the CIBA material, when oxygen gas was bled into the vacuum system during the first pass, the carbon content was lower.

The metallic impurities excepting Ta and W in the starting materials were reduced by the EBFZM. In addition, they were further reduced during the high-temperature anneal. However, the interstitial impurity level was not apparently affected much by the anneal. In the case of the annealed oxygen-treated CIBA material, there was even an increase in the apparent interstitial impurity level, particularly carbon.

Table 12 lists the measured resistance ratios obtained on the three starting materials after various treatments. The average as-zoned resistance ratios were 302, 530, 150, and 416 for the Wah Chang, DuPont, CIBA, and CIBA with oxygen treatment, respectively. The CIBA starting material for specimens 15a and 15d had an abnormally high carbon content (114 ppm), and thus the as-zoned average ratio of about 88 was not normal for the CIBA material with the standard EBFZM schedule.

The annealing treatment increased the resistance ratio in all cases. The CIBA material that had the oxygen treatment during EBFZM had the highest resistance ratio (i.e., about 1500) after annealing at 2350°C for 5 hours in 2×10^{-9} torr vacuum. However, it should be pointed out that the high resistance ratio does not necessarily mean a low-impurity content. Table 11 shows that the high-temperature anneal had little effect upon the measured total impurity.

The resolved shear stresses at the lower yield points for $\langle 491 \rangle$ niobium single crystals deformed in tension at room temperature at a strain rate of $1.7 \times 10^{-4} \text{ sec}^{-1}$ are listed in Table 13 for the three

materials. It is evident that the annealing treatment had a profound effect upon this flow stress. With the exception of Spec. C15a, which had an anomalously high carbon starting material, the anneal decreased this flow stress for all three materials by approximately 30 to 40%. Again, it should be pointed out that the chemical analyses show that the anneal did not appreciably affect the measured impurity levels.

Table 12. Resistance Ratios of Niobium
after Various Treatments

Source	Spec. No.	Treatment	$R_{300^{\circ}\text{K}}$
			$R_{4.2^{\circ}\text{K}(15 \text{ kgauss})}$
Wah Chang	58a	Zoned	299
	58d	Zoned	304
	59a	Zoned	299
	59b	Zoned	300
	59d	Zoned	310
	59d	Zoned and Annealed	734
	58a	Zoned-Centerless Grind-Chemical Polish	230
	59a	Zoned-Centerless Grind-Chemical Polish-Anneal	722
	59b	Zoned-Centerless Grind-Chemical Polish-Anneal	727
DuPont	D12a	Zoned	533
	D12d	Zoned	534
	D13a	Zoned	519
	D13d	Zoned	534
	D13d	Zoned and Annealed	951
	D12a	Zoned-Centerless Grind-Chemical Polish	404
	D13a	Zoned-Centerless Grind-Chemical Polish-Anneal	1003
CIBA	C14a	Zoned	138
	C14d	Zoned	162
	C15a	Zoned	86
	C15d	Zoned	91
	C15d	Zoned and Annealed	111
	C14a	Zoned-Centerless Grind-Chemical Polish	113
	C15a	Zoned-Centerless Grind-Chemical Polish-Anneal	99

Table 12. (Continued)

CIBA	C20a	Zoned (oxygen)	398
	C20d	Zoned (oxygen)	445
	C21a	Zoned (oxygen)	391
	C21d	Zoned (oxygen)	429
	C21d	Zoned (oxygen) and Anneal	1512
	C20a	Zoned (oxygen)-Centerless Grind-Chemical Polish	326
	C21a	Zoned (oxygen)-Centerless Grind-Chemical Polish-Anneal	1332

Table 13. Resolved Shear Stress at the Lower Yield Point for $\langle 491 \rangle$ Niobium Single Crystals Deformed in Tension at Room Temperature at a Strain Rate of $1.7 \times 10^{-4} \text{ sec}^{-1}$.

Source	Spec.	Treatment	τ_{ly} (kg/mm ²)
Wah Chang	58a	Zoned	1.51
	59a	Zoned and Annealed	1.00
	59b	Zoned and Annealed	0.96
DuPont	D12a	Zoned	1.32
	D13a	Zoned and Annealed	0.83
CIBA	C14a	Zoned	1.88
	C15a	Zoned and Annealed	1.96
	C20a	Zoned (oxygen)	1.39
	C21a	Zoned (oxygen) and Annealed	0.94

Discussion

The results indicate that the CIBA material with oxygen treatment during EBFZM is an excellent source of high-purity niobium single crystals with a low Ta and W content. The high-temperature anneal was very effective in attaining high resistance ratios and low flow stresses. The annealed CIBA material had a flow stress (τ_{ly}) of 940 g/mm² with a resistance ratio of 1330. The results for the DuPont starting material were equally good but the higher Ta and W content (i.e., about 270-ppm Ta and 70-ppm W vs about 20-ppm Ta and 2-ppm W for the Dupont and CIBA, respectively) made it less suitable for neutron irradiation experiments. The Wah Chang niobium was least desirable as a starting material as it had about 350-ppm Ta and 270-ppm W.

The fact that a high-temperature anneal in high vacuum increases the resistance ratio and decreases the flow stress of niobium has been well documented.^{95,96} However, this effect has been attributed to a purification of the metal during the anneal, particularly a reduction in oxygen and nitrogen content, and a reduction of the dislocation density. The high-temperature anneal does reduce the dislocation density.⁹⁷ However, the chemical analyses, as shown in Table 11, indicate that the anneal does not necessarily reduce the interstitial impurity content. Figure 37 is an attempted correlation between the

⁹⁵G. Taylor and J. W. Christian, "The Effect of High Vacuum Purification on the Mechanical Properties of Niobium Single Crystals," Acta Met., 13, 1216-1218, (1965).

⁹⁶M. S. Duesbery, R. A. Foxall, and P. B. Hirsch, "The Plasticity of Pure Niobium Single Crystals," Journal de Physique, Colloque C3, Supplement au n^o 7-8, Tome 27, juillet-août 1966, C3-193.

⁹⁷R. E. Reed, H. D. Guberman, and T. O. Baldwin, "The Growth of Niobium Single Crystals with Good Crystalline Perfection," Crystal Growth, Pergamon Press, New York, 1967, 829-832.

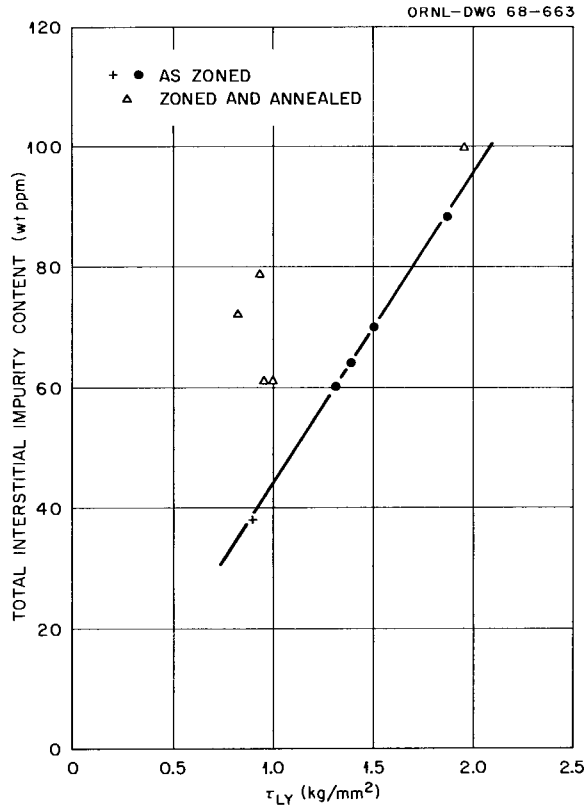


Fig. 37. Correlation of the Total Interstitial Impurity Content With Resolved Shear Stress at the Lower Yield Point for Niobium Single Crystals.

total interstitial impurity content in weight ppm and the resolved lower yield shear stress. The data point denoted by the cross is from a compression test on an as-zoned $\langle 491 \rangle$ niobium single crystal of Parma material which had a resistance ratio of 1420.⁹⁸ Apparently, there is a good correlation between the as-zoned impurity content and the flow stress regardless of the starting material. The data points from the annealed crystals do not correlate at all.

⁹⁸R. E. Reed, "Niobium: Purification and Perfection," Radiation Metallurgy Section Solid State Division Progress Report for Period Ending January 1967, ORNL-4097, 20, (1967).

Figure 38 is an attempted correlation between the resistance ratio and the flow stress. The curve is again drawn through the data for the as-zoned material. However, in this case the data from the annealed specimens show a better correlation and fall near or on the curve. Again, the various Ta and W contents of the starting materials do not seem to appreciably affect the results.

From the correlation in Fig. 38, it can be tentatively concluded that when the interstitial impurity atom is distributed such that it is an effective electron scattering center, it is also best distributed to hinder the initiation of plastic flow, as measured by the lower yield stress. However, from Fig. 37 it can be concluded that the total interstitial impurity content does not correlate well with the flow stress. Evidently, the type of distribution of the impurity atoms is an important factor. Thus, the annealed crystals had a lower percentage of the total impurity content acting as effective electron scattering centers.

It is not clear just what type of distribution of the impurity atom would be an effective electron scattering center and also hinder the initiation of plastic flow. Complete interstitial solid solution of the impurity may have this effect as this type of distribution would have the largest electron scattering cross section. Also, this distribution could offer the largest resistance to the operation of dislocation sources. Complete interstitial solid solubility of the impurities could also reduce the number of sources available. Both of these cases would raise the stress needed to initiate plastic flow. The annealing treatment could then be assumed to reduce the amount of impurity content which is in interstitial solid solution.

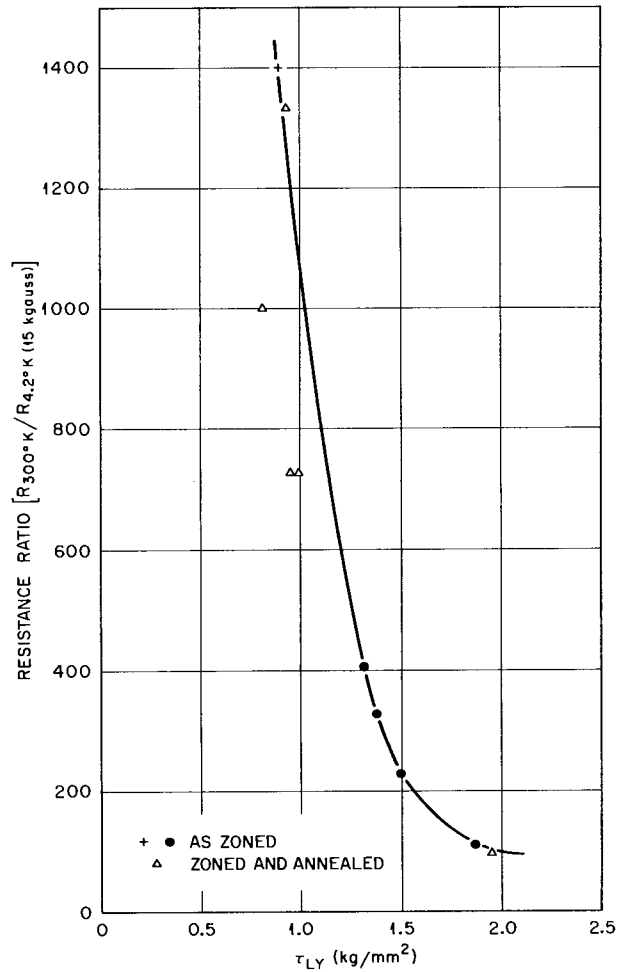


Fig. 38. Correlation of the Resistance Ratio with the Resolved Shear Stress at the Lower Yield Point for Niobium Single Crystals.

The characteristic thermal history of a point on the specimen after the EBFZM treatment would be a total amount of time near the melting point of about 3 minutes followed by a slow cool. The thermal history of the annealed specimens would be a total time of 5 hours at a temperature of 100°C below the melting point followed by a fast cool. The difference in the cooling rates is estimated to be a factor of 15. Unfortunately, such thermal histories would be expected to give just the opposite relative amounts of interstitial impurities in solid solution,

as needed to explain the data. A long time high-temperature anneal followed by a fast cool would be expected to result in more interstitial impurities in solid solution than a short time anneal followed by a slower cooling rate. Thus, perhaps some other type of impurity distribution is effective, such as clustering, formation of coherent precipitates, etc. Interaction of impurities with the dislocation substructure could also be a possibility.

Another interesting detail is apparent in Table 12. Here, the centerless ground tensile specimen after chemical polishing so that all evidence of cold work was removed (as measured by the back reflection Laue x-ray technique) exhibited resistance ratios lower than the as-zoned rods. Even annealing such a tensile specimen did not raise the resistance ratio to the level of an as-zoned and annealed specimen. The lower ratio of the chemically polished specimens could be due to the presence of hydrogen charged into the specimen during polishing. Also, residual cold work could be responsible. The fact that the high-temperature anneal does not return the resistance ratio fully to the as-zoned and annealed value may indicate that the grinding operation damages the entire cross section of the sample and the anneal does not entirely remove this effect. However, such an anneal would be expected to remove any hydrogen.

Conclusions

1. The CIBA dendritic powder was the most suitable starting material for producing high-purity niobium single crystals by EBFZM.

2. A high-temperature anneal in high vacuum will greatly increase the resistance ratio and lower the flow stress of the niobium.

3. The effect of the anneal may be a redistribution of the interstitial impurities rather than a purification.



INTERNAL DISTRIBUTION

- | | | | |
|--------|-------------------------------|------|----------------------------------|
| 1-3. | Central Research Library | 70. | W. D. Compton (consultant) |
| 4-5. | ORNL - Y-12 Technical Library | 71. | T. F. Connolly |
| | Document Reference Section | 72. | J. H. Coobs |
| 6-25. | Laboratory Records Department | 73. | J. A. Cox |
| 26. | Laboratory Records, ORNL R.C. | 74. | J. H. Crawford, Jr. (consultant) |
| 27. | ORNL Patent Office | 75. | J. C. Crump |
| 28. | M. M. Abraham | 76. | F. L. Culler |
| 29. | G. M. Adamson, Jr. | 77. | J. E. Cunningham |
| 30. | L. G. Alexander | 78. | G. V. Czjzek |
| 31. | R. W. Armstrong (consultant) | 79. | P. B. DeNee |
| 32. | W. E. Atkinson | 80. | J. H. DeVan |
| 33. | Robert Bakish (consultant) | 81. | D. A. Douglas, Jr. |
| 34. | T. O. Baldwin | 82. | Z. El Saffar |
| 35. | J. H. Barrett | 83. | J. H. Erwin |
| 36. | S. E. Beall | 84. | G. W. Glack |
| 37. | R. J. Beaver | 85. | J. L. Fowler |
| 38. | P. R. Bell | 86. | A. P. Fraas |
| 39. | M. Bender | 87. | J. H. Frye, Jr. |
| 40. | W. T. Berg | 88. | J. L. Gabbard |
| 41. | R. G. Berggren | 89. | W. B. Gauster |
| 42. | Carla Bertocci (consultant) | 90. | H. A. Gersch (consultant) |
| 43. | U. Bertocci | 91. | G. Gilat |
| 44. | J. O. Betterton, Jr. | 92. | J. H. Gillette |
| 45-46. | D. S. Billington | 93. | J. J. Gilman (consultant) |
| 47. | H. Birnbaum (consultant) | 94. | R. J. Gray |
| 48. | A. L. Boch | 95. | W. R. Grimes |
| 49. | E. G. Bohlmann | 96. | H. D. Guberman |
| 50. | E. S. Bomar | 97. | J. P. Hammond |
| 51. | B. S. Borie | 98. | W. O. Harms |
| 52. | C. J. Borkowski | 99. | C. S. Harrill |
| 53. | G. E. Boyd | 100. | M. R. Hill |
| 54. | M. A. Breazeale (consultant) | 101. | N. E. Hinkle |
| 55. | M. A. Bredig | 102. | D. K. Holmes |
| 56. | R. B. Briggs | 103. | A. S. Householder |
| 57. | F. R. Bruce | 104. | J. P. Howe (consultant) |
| 58. | W. E. Brundage | 105. | J. T. Howe |
| 59. | C. T. Butler | 106. | A. P. Huber (K-25) |
| 60. | N. Cabrera (consultant) | 107. | L. D. Hulett |
| 61. | J. W. Cable | 108. | H. Inouye |
| 62. | J. V. Cathcart | 109. | L. H. Jenkins |
| 63. | Y. Chen | 110. | R. J. Jones |
| 64. | R. O. Chester | 111. | W. H. Jordan |
| 65. | H. R. Child | 112. | G. W. Keilholtz |
| 66. | G. W. Clark | 113. | M. T. Kelley |
| 67. | J. W. Cleland | 114. | R. H. Kernohan |
| 68. | A. M. Clogston (consultant) | 115. | R. F. Kimball |
| 69. | R. R. Coltman | 116. | E. M. King |

117. C. E. Klabunde
118. F. A. Kocur
119. J. S. Koehler (consultant)
120. W. C. Koehler
121. R. B. Korsmeyer
122. J. A. Krumhansl (consultant)
123. J. A. Lane
124. C. E. Larson
125. G. Leibfried (consultant)
126. A. B. Lewis
127. R. S. Livingston
128. A. L. Lotts
129. T. S. Lundy
130. H. G. MacPherson
131. G. Mazzone
132. R. W. McClung
133. H. C. McCurdy
134. D. L. McElroy
135. C. J. McHargue
136. A. Meyer
137. A. J. Miller
138. E. C. Miller
139. J. W. Mitchell (consultant)
140. H. A. Mook
141. R. M. Moon, Jr.
142. K. Z. Morgan
143. C. M. Nelson (consultant)
144. R. M. Nicklow
145. T. S. Noggle
146. A. S. Nowick (consultant)
147. O. S. Oen
148. S. M. Ohr
149. A. R. Olsen
150. V. Pare
151. P. Patriarca
152. M. L. Picklesimer
153. J. C. Pigg
154. H. Pomerance
155. J. W. Prados
156. L. J. Raubenheimer
157. J. K. Redman
158. R. E. Reed
159. C. C. Robinson
160. M. T. Robinson
161. J. R. Russell
162. H. W. Savage
163. O. E. Schow
164. J. L. Scott
165. S. T. Sekula
166. F. A. Sherrill
167. E. D. Shipley
168. W. A. Sibley
169. R. H. Silsbee (consultant)
170. O. Sisman
171. G. M. Slaughter
172. L. Slifkin
173. G. P. Smith
174. H. G. Smith
175. A. H. Snell
176. E. Sonder
177. A. L. Southern
178. F. Specht
179. J. T. Stanley
180. J. O. Stiegler
181. W. J. Stelzman
182. B. G. Streetman
183. A. Taboada
184. E. H. Taylor
185. L. C. Templeton
186. A. S. Tetelman (consultant)
187. G. T. Trammell (consultant)
188. D. B. Trauger
189. R. P. Tucker
190. David Turnbull (consultant)
191. H. A. Ullmaier
192. D. Walton
193. C. C. Webster
194-294. M. S. Wechsler
295. R. A. Weeks
296. A. M. Weinberg
297. J. R. Weir, Jr.
298. R. D. Westbrook
299. G. D. Whitman
300. E. P. Wigner (consultant)
301. M. K. Wilkinson
302. F. E. Williams (consultant)
303. G. C. Williams
304. J. M. Williams
305. R. O. Williams
306. W. R. Willis (consultant)
307. J. C. Wilson
308. M. C. Wittels
309. E. O. Wollan
310. R. F. Wood
311. J. R. Woodyard
312. H. L. Yakel
313. F. W. Young
314. Gale Young
315. W. H. Young

EXTERNAL DISTRIBUTION

- 316. C. M. Adams, Jr., Massachusetts Institute of Technology
- 317. S. Amelinckx, Solid State Physics Department, C.E.N., Mol-Donk, Belgium
- 318. P. Baruch, Laboratoire de Physique, Ecole Normale Supérieure, Paris V, France
- 319. V. B. Bhanot, Physics Department, Panjab University, Chandigarh-3, India
- 320. T. H. Blewitt, Argonne National Laboratory
- 321. Boeing Airplane Company
- 322. R. O. Bolt, California Research Corporation, Richmond
- 323. J. A. Brinkman, North American Aviation Science Center, Thousand Oaks, California
- 324. H. Brooks, Harvard University, Cambridge, Massachusetts
- 325. R. B. Burlin, Atomic Energy Commission, Washington
- 326. J. G. Castle, Jr., Physics Department, Westinghouse Electric Corporation, Research Laboratories, Pittsburgh, Pennsylvania
- 327. R. A. Charpie, Union Carbide Corporation, New York
- 328. E. D. Clavert, U. S. Bureau of Mines, P. O. Box 492, Albany, Oregon
- 329. C. B. Cooper, Department of Physics, University of Delaware Newark, Delaware
- 330-331. D. F. Cope, RDT Site Office (Oak Ridge National Laboratory)
- 332. D. Dautreppe, CEN-B, Boite Postale No. 269, Grenoble, France
- 333. J. Diehl, Max Planck Institut für Metallforschung, Seestrass 75, Stuttgart N, Germany
- 334. H. D. Dietze, Lehrstuhl für Reaktorwerkstoffe, Technische Hochschule, Aachen, Germany
- 335. J. F. Elliott, Massachusetts Institute of Technology
- 336. L. B. Emler, Union Carbide Corporation, New York
- 337. N. Engel, Georgia Institute of Technology
- 338. H. Y. Fan, Solid State Physics Department, Purdue University, Lafayette, Indiana
- 339. H. B. Finger, Atomic Energy Commission, Washington
- 340. J. D. Fleming, Georgia Institute of Technology
- 341. V. D. Frechette, Alfred University
- 342. J. Friedel, Physique des Solides, Faculté des Sciences d'Orsay, Orsay, France
- 343. Angelo Giambusso, Atomic Energy Commission, Washington
- 344. R. G. Gilliland, Massachusetts Institute of Technology
- 345. R. H. Gillette, European Research Associates, Brussels, Belgium
- 346. J. L. Gregg, Bard Hall, Cornell University
- 347. W. W. Grigorieff, Assistant to the Executive Director, Oak Ridge Associated Universities
- 348. R. F. Hehmann, Case Institute of Technology
- 349. J. Hitch, Office of Isotope Development, AEC, Washington
- 350. E. E. Hoffman, General Electric, Cincinnati, Ohio
- 351. H. Huntington, Department of Physics, Rensselaer Polytechnic Institute, Troy, New York
- 352. J. R. Johnson, Minnesota Mining and Manufacturing Company, St. Paul, Minnesota

353. L. K. Keys, General Electric, Cincinnati, Ohio
 354. C. Kikuchi, University of Michigan, Willow Run Laboratory, Ann Arbor, Michigan
 355. O. C. Kopp, University of Tennessee, Knoxville
 356. J. Korringa, Ohio State University
 357-358. W. J. Larkin, Atomic Energy Commission, Oak Ridge
 359. Benjamin Lax, Lincoln Laboratory, Lexington, Massachusetts
 360. C. Lehmann, KFA-Werkstoffinstitut, Julich, Germany
 361. R. I. Leininger, Battelle Memorial Institute, Columbus, Ohio
 362. A. B. Lidiard, AERE, Harwell, England
 363. J. J. Lombardo, NASA, Lewis Research Center
 364. W. M. Lomer, AERE, Harwell, England
 365. W. C. Mallard, Emory University, Atlanta, Georgia
 366. W. D. Manly, Union Carbide Corporation, Stellite Division
 367. W. Marshall, AERE, Harwell, England
 368. R. S. Mateer, University of Kentucky
 369. P. W. McDaniel, Division of Research, USAEC, Washington
 370. A. Merlini, Solid State Physics Department, C.C.R.-EURATOM, Ispra (Varese), Italy
 371. R. M. Milton, Linde Division, Union Carbide Corporation, P. O. Box 44, Tonawanda, New York
 372. Peter Murray, AERE, Harwell, England
 373. R. R. Nash, NASA, Washington
 374. E. F. Nippes, Rensselaer Polytechnic Institute
 375. H. M. Otte, Martin Company, Orlando, Florida
 376. R. E. Pahler, Atomic Energy Commission, Washington
 377. R. M. Parke, MAB, National Academy of Science, Washington
 378. J. Pheline, Centre d'Etudes Nucleaires de Saclay
 379. J. M. Prosser, Atomic Energy Commission, Washington
 380. H. B. Rahner, Savannah River Operations
 381. R. E. Reed-Hill, University of Florida
 382. Research and Development Division, AEC, ORO
 383. F. N. Rhines, University of Florida
 384. A. E. Ruark, Atomic Energy Commission, Washington
 385. H. Saito, Department of Physics, College of General Education, Osaka University, Osaka, Japan
 386. A. F. Saturno, University of Tennessee, Knoxville
 387. R. W. Schroeder, NASA, Lewis Research Center
 388. R. J. Schuttler, Service SEPP, CEN/FAR (Ford de Chatillion), Boite Postale 6, Fontenay-aux-Roses (Seine), France
 389. F. C. Schwenk, Atomic Energy Commission, Washington
 390. A. Seeger, Max Planck Institut fur Metallforschung, Seestrasse 75, Stuttgart N, Germany
 391. F. Seitz, University of Illinois, Urbana, Illinois
 392. W. W. Shaver, Corning Glass Works, Corning, New York
 393. A. A. Shoudy, Atomic Power Development Associate, Inc.
 394. J. M. Simmons, Division of Reactor Development, AEC, Washington
 395. O. C. Simpson, Argonne National Laboratory
 396. E. E. Sinclair, Atomic Energy Commission, Washington
 397. A. Sosin, Atomics International, Canoga Park, California
 398. E. E. Stansbury, University of Tennessee, Knoxville
 399. D. K. Stevens, Materials and Metallurgy Branch, AEC, Washington

400. G. L. Stiehl, Convair Division of General Dynamics Corporation
San Diego, California
401. R. Street, Department of Physics, Monash University, P. O. Box
92, Clayton, Victoria, Australia
402. J. A. Swartout, 270 Park Avenue, New York 17, New York
403. D. O. Thompson, North American Aviation Science Center,
Thousand Oaks, California
404. J. B. Trice, Military Space Vehicle Department, General Electric
Company, Philadelphia, Pennsylvania
405. T. J. Turner, Department of Physics, Wake Forest College,
Winston-Salem, North Carolina
406. A. Van Echo, Atomic Energy Commission, Washington
407. G. H. Vineyard, Brookhaven National Laboratory, Upton, Long
Island, New York
408. J. B. Wagner, Massachusetts Institute of Technology
409. G. D. Watkins, General Electric Research Laboratories,
Schenectady, New York
410. Watt Webb, Union Carbide Metals
411. J. Weertman, Northwestern University
412. G. W. Wench, Atomic Energy Commission, Washington
413. Westinghouse Electric Corporation, Research Laboratories,
Pittsburgh, Pennsylvania
414. M. J. Whitman, Atomic Energy Commission, Washington
415. C. H. T. Wilkins, University of Alabama
416. Manfred Wuttig, University of Missouri, Rolla, Missouri
417. C. D. Yost, ARPA, Pentagon, Washington, D. C.
418. R. A. Young, Georgia Institute of Technology, Atlanta, Georgia
- 419-683. Given distribution as shown in TID-4500 under Metals, Ceramics,
and Materials category (25 copies - CFSTI)